

공학석사 학위논문

직렬연결된 배터리 구조에서 개별 셀
노화특성을 고려한 실시간 SOC/SOH
추정기법

**Online SOC/SOH Estimation for Individual Cells
in the Battery String Considering the Aging Effect**

울산대학교 대학원
전기전자컴퓨터공학과
NGOC-THAO PHAM

직렬연결된 배터리 구조에서 개별 셀
노화특성을 고려한 실시간 SOC/SOH
추정기법

**Online SOC/SOH Estimation for Individual Cells in
the Battery String Considering the Aging Effect**

지도교수 최성진

이 논문을 공학석사 학위논문으로 제출함

2022년 12월

울산대학교 대학원
전기전자컴퓨터공학과
NGOC-THAO PHAM

NGOC-THAO PHAM 의 공학석사학위 논문을 인준함

심사위원장

전태원



심사위원

최성진



심사위원

권성오



울산대학교 대학원
전기전자컴퓨터공학과

2022 년 12 월

UNIVERSITY OF ULSAN

**Online SOC/SOH Estimation for Individual Cells
in the Battery String Considering the Aging Effect**

by

NGOC THAO-PHAM

Supervisor: Professor SUNG-JIN CHOI

A dissertation submitted in partial fulfillment of
the requirements for the degree of Master of Science

in the

Department of Electrical, Electronic and Computer

Engineering

University of Ulsan

December 2022

This certifies that the dissertation of NGOC-THAO PHAM is
approved by:

Committee Chair: **Professor Tae-Won Chun**

Signature:



Committee Member: **Professor Sung-Jin Choi**

Signature:



Committee Member: **Professor Sungoh Kwon**

Signature:



Department of Electrical, Electronic, and Computer Engineering

University of Ulsan

December 2022

Acknowledgements

First of all, I would like to express my gratitude to my supervisor, professor Choi Sung Jin, for insightful advice, support, and inspiration in shaping the research direction and research methodology during my master's study at the University of Ulsan. I am delighted to complete my master's study under his direction.

Next, I would like to thank Brain Korea 21 Plus (BK21+) and the National Research Foundation of Korea (NRF). I would also like to thank my lab colleagues in the Energy Conversion Circuits Laboratory (ECCL) for their support, help, and memorable moments in my course. I especially would like to thank Mr. La Phuong Ha and Mr. Nguyen Nguyen Anh for their discussions, encouragement, and support whenever I get in trouble.

Last but not least, I would like to express my deep and sincere to my parents and my friends for their caring, loving, encouragement, and support.

Abstract

Nowadays, Lithium-ion battery is widely utilized in various fields: electric vehicles (EV), energy storage system (ESS), and portable devices. Depending on the usage requirements, a hundred or even a thousand battery cells are serially connected in the battery power systems. The aging of cells during the operation leads to inconsistency between the cells, which is reduce the reliability and safety of the system. Besides, the battery pack will be replaced when its state of health (SOH) is below 80%. Due to the economic and environmental issues, the retired battery pack is reutilized as a second life battery for the systems that require less performance, eg: BESS. The batteries in a pack should be monitored or classified for other purposes. Therefore, the state of health and state of charge (SOC) estimation of the individual cell are extremely necessary.

In previous battery estimation, SOC is estimated by the column counting method and OCV method. These methods are easy to implement and require a low computational burden. However, the estimation accuracy is not only dependent on the error accumulating in the current sensor but also sensitive to temperature and aging. The data-driven method can obtain a high accuracy of SOC estimation without the battery model. Nevertheless, this method requires numerous data and can be limited by computational burden. Although Kalman-filter-based battery state estimation is one of the most popular methods, it is sensitive to the accuracy of the battery model parameters and difficult to be applied to every cell.

This work proposes an online cell-by-cell SOC/SOH estimation method to mitigate this limitation. The aging patterns of the individual cells are predicted by introducing a combination of a switch-matrix flying capacitor and electrochemical impedance spectroscopy (EIS) model parameter scanning techniques. Accordingly, the accuracy of the SOC estimation for individual cells is enhanced. The proposed method is verified by a real-time simulation platform, where the SOC and SOH levels of the cells are individually estimated within a 1.63% RMSE.

Keywords battery cell, battery estimation, battery model, EIS, EKF calibration, integrated impedance measurement

Table of contents

List of figures	xi
List of tables	xii
Nomenclature	xiii
1 Introduction	1
1.1 Motivation and problem description	1
1.2 Objectives and contributions	3
1.3 Thesis Organization	5
2 Battery model identification and SOC/SOH estimation	7
2.1 Overview	7
2.2 Conventional model identification	8
2.3 Conventional SOH/SOC estimation	11
2.4 Switched capacitor equalizer	12
2.5 Conclusion	13
3 Proposed online battery model identification	14
3.1 Circuit structure	15
3.2 EIS algorithm	20
3.2.1 Start and end time point strategy (S-ETPS)	21
3.2.2 Multiple time point strategy (MTPS)	23
3.3 Conclusion	26
4 Proposed SOC/SOH estimation method using online model identification	27
4.1 Extended Kalman filter formula	27
4.2 SOH estimation	29
4.3 SOC estimation	33
4.4 Conclusion	35

5	Experimental verification	36
5.1	Battery data set	37
5.2	Validation of EIS identification	40
5.3	Validation of SOH/SOC estimation	46
5.4	Conclusion	48
6	Conclusion and future work	53
6.1	Conclusion	53
6.2	Future work	54
	References	57

List of figures

1.1	Proposed SOH/SOC estimation method	4
2.1	Sinusoidal injection method	9
2.2	Genetic algorithm	10
2.3	Switched capacitor equalizer	13
3.1	Integrated measurement circuit	16
3.2	Integrated measurement circuit detail	17
3.3	Control flowchart of the EIS-model identification for series-connected battery cells	18
3.4	An illustration of the Thévenin model	19
3.5	Equivalent circuit in s-domain	20
3.6	Theoretical waveforms S-ETPS	22
3.7	Theoretical waveforms MTPS	23
3.8	Exponential curve fitting theory	25
4.1	Battery impedance change during aging	31
4.2	SOC-OCV change during aging	32
4.3	SOC estimation without model calibration at 100% and 90% SOH	32
4.4	Relationship between SOH and R_t	33
5.1	Battery data set test set up	39
5.2	Flow chart of the processing test	41
5.3	Real time simulation result of voltage and current waveforms	42
5.4	Cole–Cole plot of the impedance	43
5.5	SOC estimation result at 97.75% SOH	50
5.6	SOC estimation result at 92.36% SOH	51
5.7	SOC estimation result at 91.3% SOH	52

List of tables

5.1	Battery Samsung INR18650-29E specifications	38
5.2	Model-parameter Identification Results of S-ETPS	44
5.3	Model-parameter Identification Results of MPTS	45
5.4	Model-parameter Identification Results for 3 cells	49
5.5	SOH estimation result by proposed method	50

Nomenclature

Acronyms

SLB	Second life battery
S-ETPS	Start and end time point strategy
MTPS	Multiple time points strategy
LUT	Look up table
RMSE	Root mean square error
BMS	Battery management system
EKF	Extended Kalman filter
EIS	Electrochemical impedance spectroscopy
SOC	State of charge
SOH	State of health
EV	Electric vehicle
BESS	Battery energy storage system
ML	Machine learning
DL	Deep learning

Chapter 1

Introduction

1.1 Motivation and problem description

As a more environmentally friendly method of transportation, battery electric vehicles (EVs) are attracting a lot of global attention [1]. The battery energy storage system (BESS) effectively overcomes the fossil fuel crisis and environmental pollution, considered the major hurdle for the automobile industry [2]. The market share of BESS is growing faster [3] due to their advantages such as lightweight, fast charging, high energy density, low self-discharge, and long lifespan [4]. In recent electric vehicle development, a new cell-packing structure is emerging such as a cell-to-pack technology that directly embeds the cells in the pack and eliminates modules. Besides, the battery pack is not only an enclosure but also a part of the vehicle body structure, so-called as a cell-to-vehicle solution. Therefore, the number of cells connected in series is further increasing.

Usually, the battery cells are screened, so as to have similar characteristics before being grouped into a module or a pack [5]. However, it ensures the uniform performance of the cells only in the first few operation cycles. It is because individual cells are operating in different

1.1 Motivation and problem description

cooling profiles and the aging patterns of the cells are dissimilar from each other. Therefore, estimation results for the whole battery module or pack mostly fail to represent the state of individual cells [6]. Since the aging patterns of the individual cells are dissimilar [7], the mismatch in the battery characteristics can make the series string suffer from over-charging and over-discharging [8].

This kind of problem becomes more severe in the second-life battery system, where the retired battery pack from an EV is reused for BESS application. At this time, individual cell characteristics are not as uniform as the new one [9]. For that reason, the battery state of individual cells should be monitored by considering the aging characteristics of the individual cell rather than a whole battery module or pack.

Since the state of charge level only can be estimated based on the battery voltage, current, and temperature [10], battery state estimation techniques are actively investigated [11, 12]. For example, the Coulomb counting method estimates the SOC level of the cells by counting the amount of charge that flows into or out of the cell. Due to its simplicity, it becomes the most popular in industrial applications [13, 14]. Additionally, data-driven approaches such as artificial intelligence-based techniques are becoming another trend. The machine learning (ML) and the deep learning (DL) algorithms can accurately estimate the SOC level of the cells [15]. However, the ML-based methods require a large dataset to train the model before operation on site and the DL-based methods show a large estimation error in the first few cycles showing a risk in safety. Besides, the required computation time is too much to gain the practical feasibility and meet the cost requirements.

On the other hand, model-based methods can estimate the SOC level with high accuracy and a low computation time [16]. For example, Kalman-filter-based battery state estimation

1.2 Objectives and contributions

is one of the most popular methods. However, it is reported that they are sensitive to the accuracy of the battery model parameters. The impact of battery aging on the estimation accuracy is mostly neglected even though it is shown to be significant [17]. To ensure the estimation accuracy, the battery model parameters should be online monitored to reconfigure the state space model.

In recent years, many studies apply machine learning to optimize the EKF algorithm. In [18, 19], the authors utilize reinforcement learning to modify the parameters of EKF. Although this approach could gain some impressive results because of self-learning ability based on real collected data, it also has the limitations of data-driven methods such as a variety of training data, a long training time, and high computation burden.

1.2 Objectives and contributions

In order to solve the problem mentioned in the previous section, this work proposes an effective online cell-by-cell state-of-charge SOC/state-of-health SOH estimation method for the series string. The impedance degradation of the cells is detected by utilizing an online identification method. While the SOH is estimated based on the impedance degradation, the model parameters of the individual cell are also calibrated. Besides, an EKF algorithm is used to estimate the SOC level from the updated state space model and open circuit voltage information.

The parameter reconfiguration process of one cell is demonstrated in Fig. 1.1. In the EIS model identification block, the model parameters of the cell are identified. The proposed method is developed for a switch-matrix flying capacitor circuit that is connected in turns to the individual cells. Most of the equivalent model parameters of the cells can be estimated

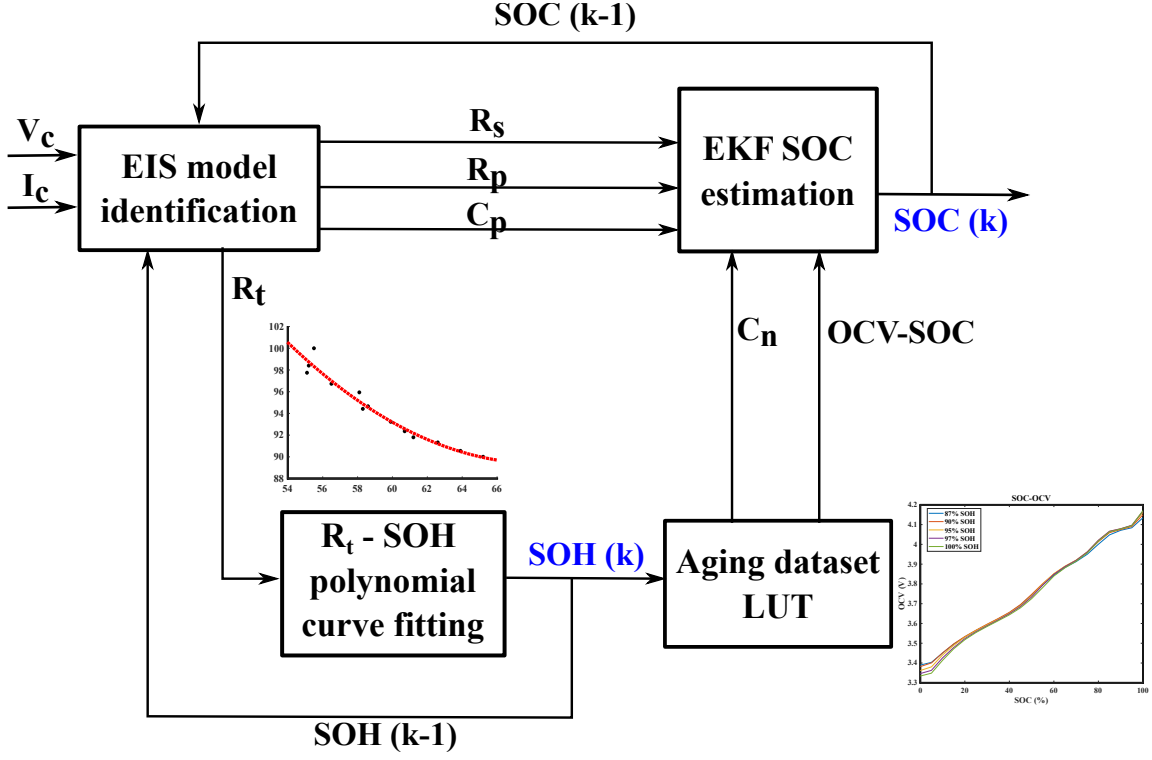


Fig. 1.1 Proposed SOH/SOC estimation method

based on the charge transfer theory of the switched capacitor circuit. Accordingly, the EIS model is utilized to update the state space model for SOC estimation. The SOH level is a function of R_t , which can be derived by applying the polynomial curve fitting technique. Therefore, the SOH level is estimated directly from the measured R_t . Thenceforth, the impedance degradation is detected to interpolate the SOH level. The corresponding OCV–SOC relationship and the state space model of the EKF are reconfigured based on the estimated SOH level. In virtue of the switch-matrix, the estimation process can be implemented for the individual cells one by one. Furthermore, the proposed method is the online method, which is applied based on the existing capacitor equalizer without detaching the battery pack.

1.3 Thesis Organization

The thesis includes the chapters listed below,

Chapter 1: INTRODUCTION - The research motivation and objective of Li-ion battery technology for SOC is elaborately discussed in the section. At the time, the problem formulation research objective and implementation technique of this thesis are briefly explained.

Chapter 2: BATTERY MODEL IDENTIFICATION AND SOH/SOC ESTIMATION - The chapter mentions the overview of battery identification and SOH/SOC estimation. The definition and conventional method are included, as drawbacks of each method, and switched capacitor equalizer.

Chapter 3: PROPOSED ONLINE BATTERY MODEL IDENTIFICATION - the integrated circuit structure is analyzed. This chapter proposed two current sampling strategies to determine the battery parameter.

Chapter 4: PROPOSED SOH/SOC METHOD USING ONLINE MODEL IDENTIFICATION - Apply battery model calibration for SOC estimation. This chapter introduces how to update the EKF state equation based on online model identification and SOH value.

Chapter 5: EXPERIMENTAL VERIFICATION - The experimental conducting, data collection tactics, parameter identification results, and simulation verification experiments are extensively incorporated in this chapter. After then, compared the SOC with calibration to SOC without calibration is making.

Chapter 6: CONCLUSIONS AND FUTURE WORK - Summarized the entire graduation thesis design work, reviewed the all contents and the difficulties encountered in the design process, and proposed some improvement measures.

Chapter 2

Battery model identification and SOC/SOH estimation

2.1 Overview

The rising trend of transportation electrification is growing fast in recent years. Unfortunately, bringing up the rear is a significantly retired battery pack of EV, which is forecasted to be up to 120GWh by 2030 [20]. Since the labor cost for material recycling is too high that prevents the practical feasibility [21, 22], re-utilize the retired battery packs of EV for BESS is a more positive approach [9]. The challenge of the re-used battery applications is the performance inconsistency of the battery cells after a diligent operation in EV duration [23]. Thus, a high-performance battery management system (BMS) for individual cells is required.

Additionally, in EV and BESS, battery cells are connected in series to increase the operating voltage range. Although the characteristics of the cells are screened before assembling [3], their behaviors are getting different during the aging [5]. Thus, a high-performance

BMS for individual cells is required. In general, the SOC and SOH of the cells should be continuously monitored. Among various state estimation methods, the model-based SOC estimation techniques show the best performance on the ground of accuracy [6]. However, when it comes to system integration, most of the existing methods are only feasible for the whole battery pack. Since the impact of cell inconsistency becomes more serious due to battery aging, the estimation accuracy is significantly decreased without considering the inconsistency between the cells. Thus, the individual cells should be characterized during system operation to calibrate the coefficients of the estimator.

2.2 Conventional model identification

Various impedance measurement and model characterization methods are introduced in [24], where the sinusoidal injection is the textbook scheme for battery application as in Fig. 2.1. Should the object has a high impedance, a sinusoidal voltage signal (Potentiostatic) is injected to get a corresponding current. Hence, the magnitude and the phase angle of impedance are analyzed to estimate the parameter of the battery model. On the contrary, a sinusoidal current signal (Galvanostatic) is injected into a small impedance object to observe the corresponding voltage, and then the model-parameters are identified. Both methods have high precision, but the signal injection could lead the battery cells to overload conditions when the characteristics of the battery cells are unknown.

Besides, the sinusoidal injection method only obtain Nyquist plot of the battery. An additional method should be utilized to determined the battery model. In some commercial EIS equipment utilizing the genetic algorithm to obtain the battery model. The genetic

A sinusoidal injection

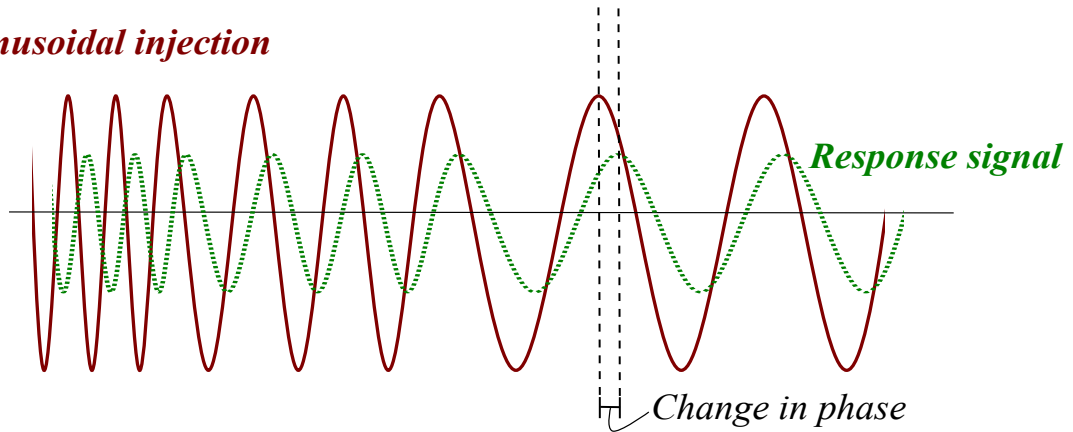


Fig. 2.1 Sinusoidal injection method

algorithm applies the same technique in data mining – it iteratively performs the selection, crossover, mutation, and encoding process to evolve the successive generation of models.

The components of genetic algorithms consist of:

Population incorporating individuals.

Encoding or decoding mechanism of individuals.

The objective function and an associated fitness evaluation criterion.

Selection procedure.

Genetic operators like recombination or crossover, mutation.

Probabilities to perform genetic operations.

Replacement technique.

Termination combination.

At every iteration, the algorithm delivers a model that inherits its traits from the previous model and competes with the other models until the most predictive model survive.

In general, this method requires a long relaxation time for the battery before each measurement to eliminate the polarization effect. Besides, the EIS identification time is

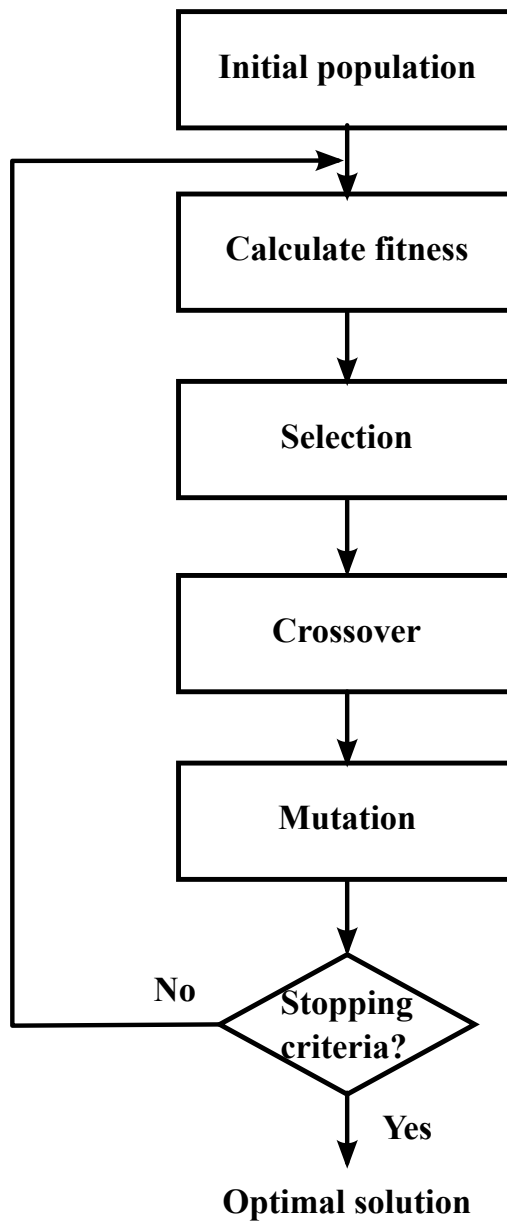


Fig. 2.2 Genetic algorithm

high due to the frequency-swept scheme. By considering the disadvantages, sinusoidal signal injection is unsuitable for the online state monitoring of BMS.

2.3 Conventional SOH/SOC estimation

According to [25] state of health (SOH) is a figure of merit of the present condition of a battery cell (or a battery module, or a battery system), compared to its ideal conditions. The unit of SOH is percent, and 100% means it is a fresh battery. Consider the capacity as an example, SOH could be defined as the ratio of the current capacity and the rated capacity given by the manufacture. Typically, the BMS will alert the user to change the batteries if the battery capacity is 80% lower than the starting value. State of charge (SOC) means the ratio of the remaining charge of the battery and the total charge while the battery is fully charged at the same specific standard condition. And the SOC is often expressed in percent, 100% means fully charged and 0% means fully discharged.

Given that the state of charge level only can be estimated based on the battery voltage, current, and temperature [10], the battery state estimation techniques are actively investigated [11, 12]. For example, the Coulomb counting method estimates the SOC level of the cells by counting the amount of charge that flows into or out of the cell. This method has become the most preferred in industrial applications due to its simplicity [13, 14]. Additionally, data-driven approaches such as artificial intelligence-based techniques are also gaining popularity. ML and DL algorithms can accurately estimate the SOC level of the cells [15, 26, 27]. However, the ML-based methods require a large dataset to train the model before operation on site, and the DL-based methods demonstrate a large estimation error in the first few cycles showing a risk in safety. Meanwhile, the required computation time is considerably long to gain practical feasibility and meet the cost requirements. On the other hand, model-based methods can estimate the SOC level with high accuracy and a low computation time [16, 28]. For example, Kalman-filter-based battery state estimation is one of the most popular methods. However,

reports indicated that these methods are sensitive to the accuracy of the battery model parameters. The influence of battery aging on the estimation accuracy is mostly neglected, even though it is significant [17, 29]. To ensure the estimation accuracy, the battery model parameters should be online monitored to reconfigure the state space model. In recent years, many studies apply machine learning to optimize EKF algorithm. In [18, 19], the authors utilize reinforcement learning to modify the parameters of EKF. Although this approach could gain some impressive results because of self-learning ability based on real collected data, it also has the limitations of data-driven methods, such as a variety of training data, a long training time, and high computation burden.

2.4 Switched capacitor equalizer

According to the structure in Fig. 2.3, one bi-directional current sensor is adopted to measure the equalization current [30]. The SOC rates of battery cells are estimated by utilizing the measured current. Based on the SOC rate of cells, the donor or receiver cell is decided to equalize the energy through a switch matrix and one capacitor. Thus, the charge is transferred directly between any cells. The equalization capacitor, C , alternately connects with each battery cell through the corresponding switches, S_{iH} and S_{iL} , in the matrix to observe the process current flowing between the host and the guest cells during the scanning time.

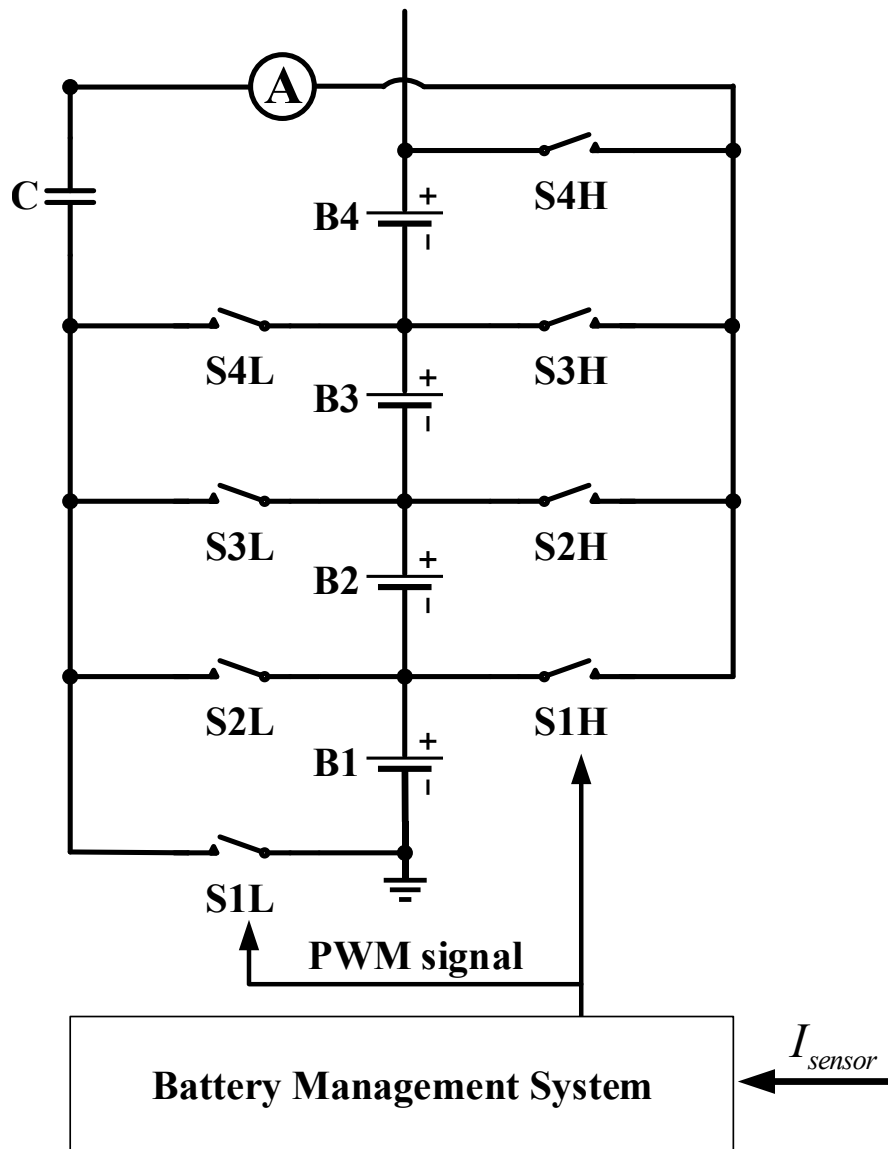


Fig. 2.3 Switched capacitor equalizer

2.5 Conclusion

The chapter mentions the overview of the issue. The definition and conventional method of battery identification and SOH/SOC estimation are included, as drawbacks of each method. And the switched capacitor equalizer is also introduced.

Chapter 3

Proposed online battery model identification

The proposed EIS-model parameters identification scheme is embedded into the existing switched-capacitor equalizer as Fig. 3.1. By the virtue of switch-matrix structure, the equalizing capacitor, C , can connect to any battery cell in the series string. When the equalizing capacitor and the battery are connected, the charge transfer process occurs. To ensure that the equalizing-capacitor is empty before each identification step, one resistor, one switch, and one voltage sensing circuit are added to the existing equalizer circuit. Because the proposed scheme utilizes the equalizing capacitor of the existing circuit, the value of capacitance is dependent on the design of the equalizer circuit. The design of switches and equalizing capacitor are provided in [30].

3.1 Circuit structure

In general, the equalization process is executed intermittently, when the battery cells are in idle mode. Accordingly, the EIS-model identification process is started before the equalization step, when the battery cells reach steady-state status. The whole identification process is described in Fig. 3.3. Before every identification step, the equalizing capacitor is fully discharged to ensure the zero initial voltage. One identification process of one cell is divided into two phases as Fig. 3.2(a). By controlling the switches, SiH and SiL , one battery cell is connected to the equalizing capacitor. As a result, the charge transferring process occurs from battery cell to the capacitor. By analyzing the capacitor voltage and current, EIS-model parameters are identified. After the identification process is finished, the equalizing capacitor is discharged by a dummy resistor, R_{dummy} , until the capacitor becomes completely discharged. Next, the identification process for the next cell is executed as Fig. Fig. 3.2(b-c). After all cells are scanned, the identification process is terminated. The obtained EIS-model parameters are utilized to calibrate the coefficients of the SOC estimator or to estimate the SOH status based on the impedance degradation. Since the EIS-model is identified after only a single charge transfer cycle, energy loss during the identification process is trivial. Besides, the impedance degradation requires a long time to occur. Thus, the EIS-model identification process is only executed intermittently and the energy loss is very low.

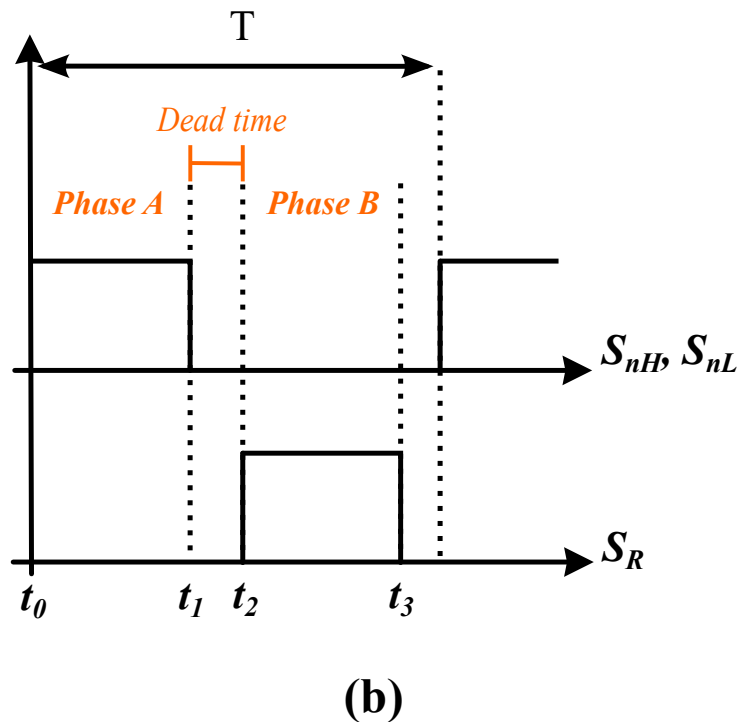
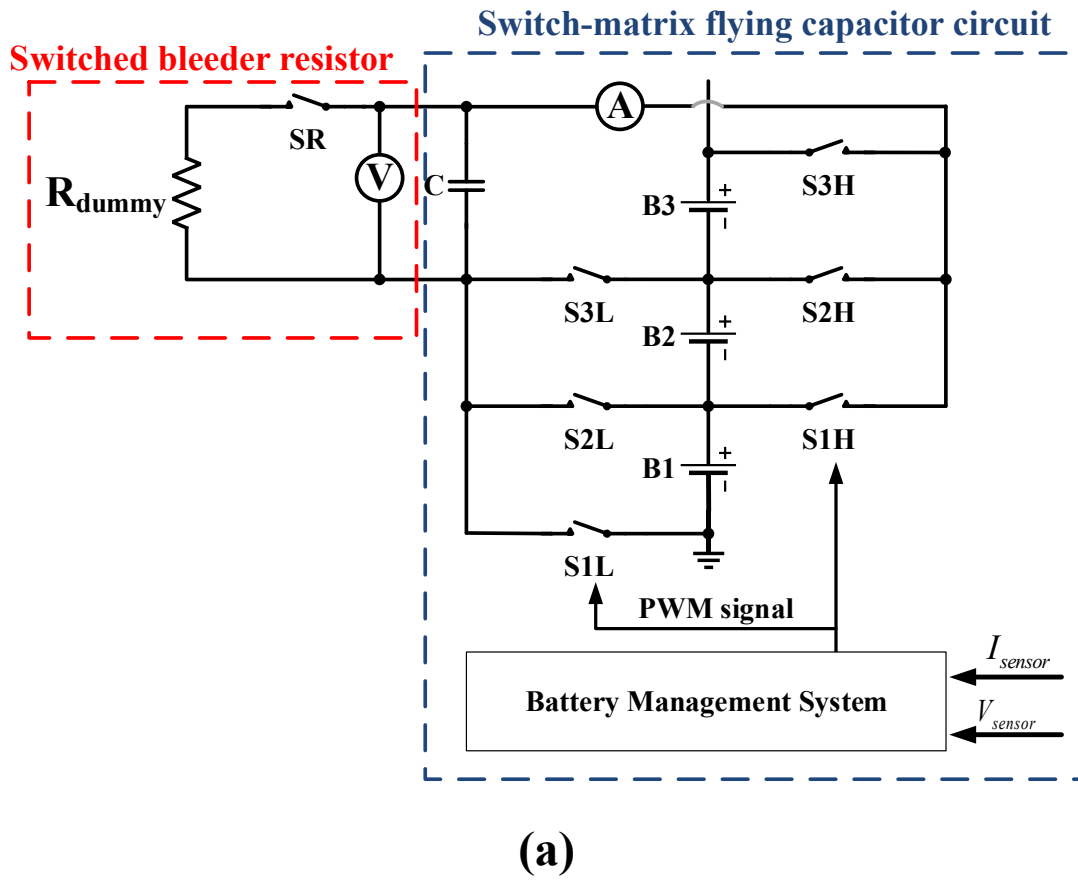


Fig. 3.1 Integrated measurement circuit: (a) overall circuit; (b) switching signal of the process

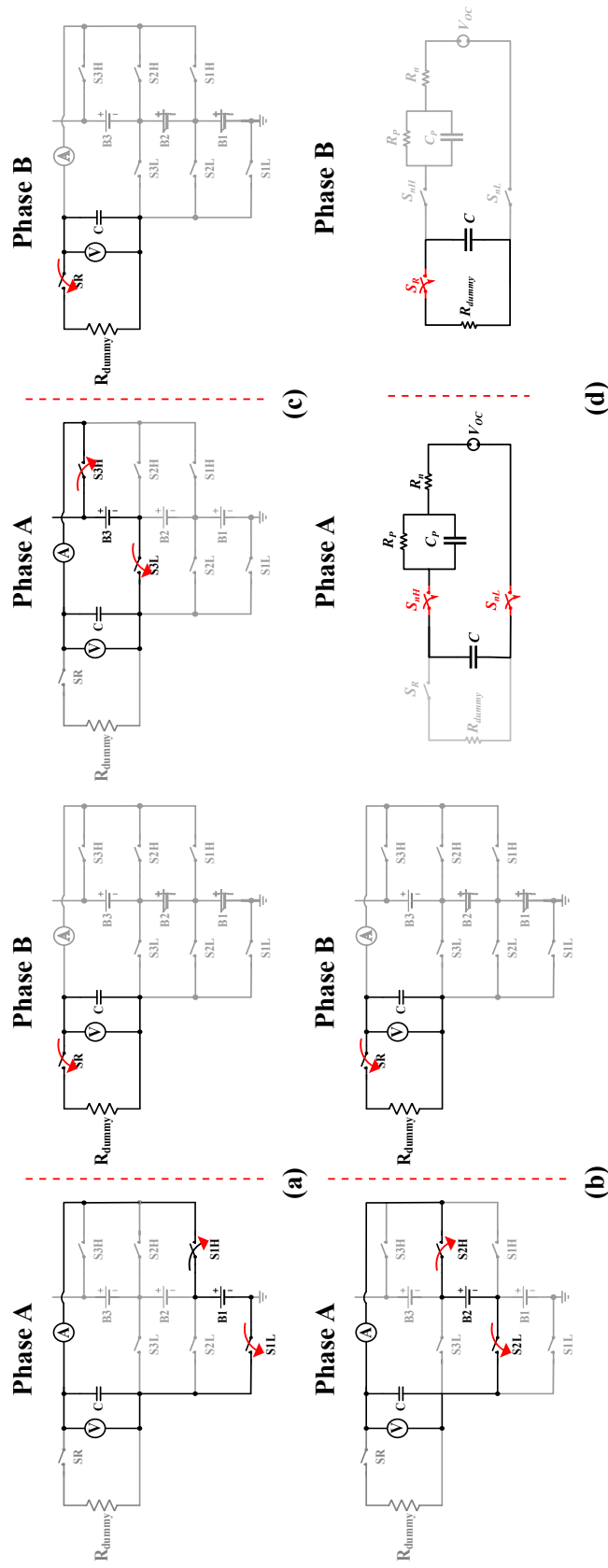


Fig. 3.2 Integrated measurement circuit: (a) measurement process of cell #1; (b) measurement process of cell #3; (c) measurement process of cell #2; and (d) equivalent circuit

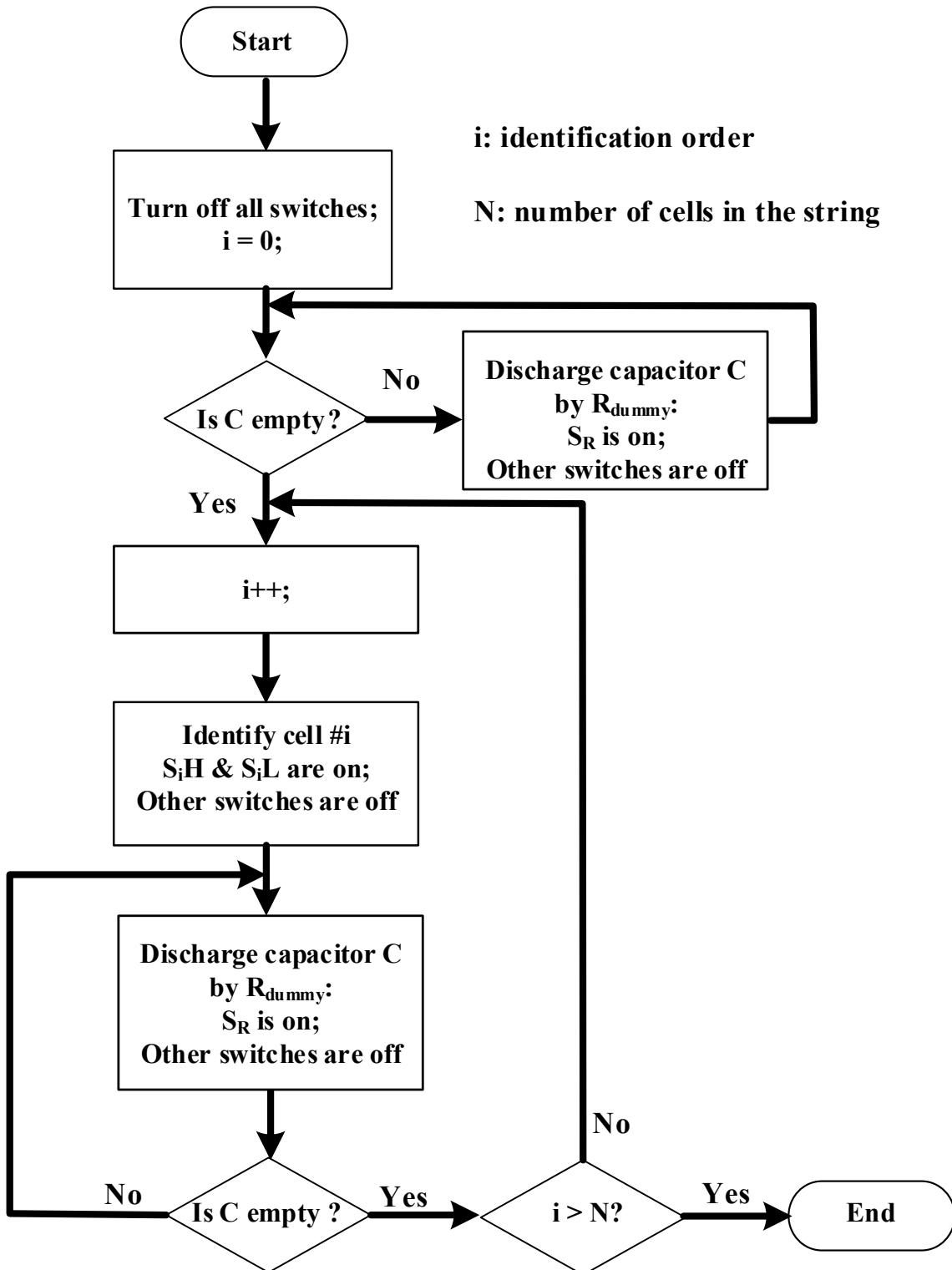


Fig. 3.3 Control flowchart of the EIS-model identification for series-connected battery cells

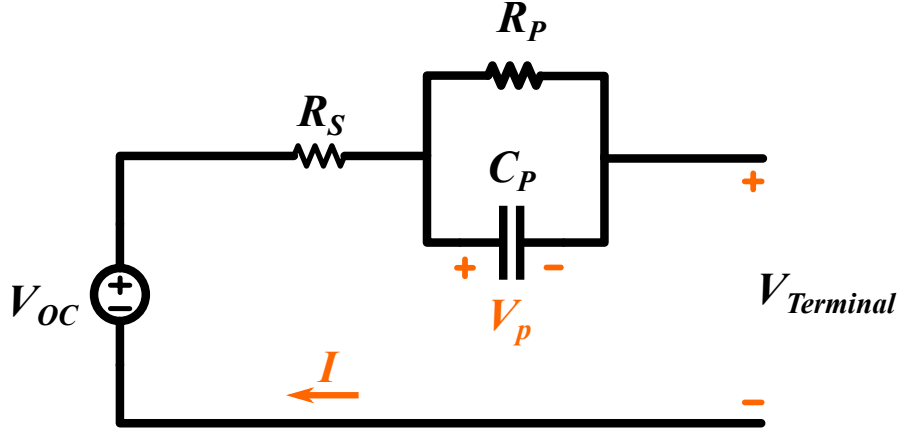


Fig. 3.4 An illustration of the Thévenin model

Although the accuracy of the conventional sinusoidal injection scheme is good, the execution time of the frequency-sweep is usually long. The proposed scheme utilizes the charge transfer process of the switched-capacitor converter to obtain the EIS-model of the battery chemical time constant that has a large. Thus, the switched-capacitor equalizer is operated below 1Hz frequency to observe the behavior of the battery impedance and reduce the execution time.

Various EIS-models of battery [31] can be used for the modeling of the charge transfer process. The high-order EIS-model can increase the accuracy of the state estimation, but the calculation of the identification becomes more complex. Considering the trade-off between the computation complexity and the estimation accuracy, the battery cell is modeled by a Thévenin model with a single R-C network as in Fig. 3.4. The identification process is divided into two phases as Fig. 3.5, where: (a) identification phase A based on the charge transfer ($t_0 \sim t_1$) and (b) capacitor discharge phase B ($t_2 \sim t_3$).

During phase A ($t_0 \sim t_1$), the switches S_{nH} and S_{nL} are turned on while S_R is kept off. By applying KCL and KVL to the model in s-domain as Fig. 3.5(a), the current flow in the

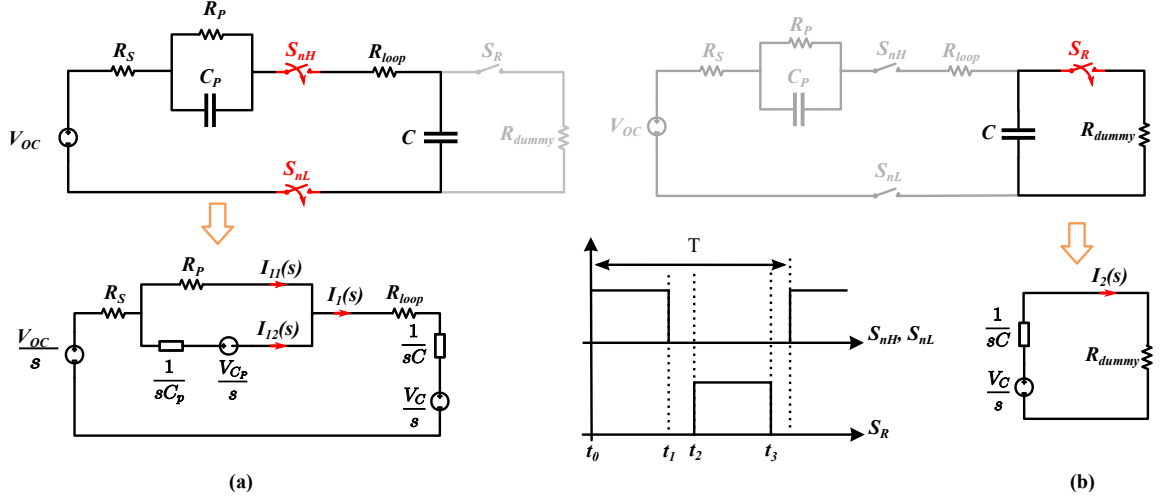


Fig. 3.5 Equivalent circuit in s-domain: (a) phase A ($t_0 \sim t_1$); (b) phase B ($t_2 \sim t_3$)

loop is calculated by

$$I_1(s) = \frac{V_{OC} - V_C}{s} \frac{1 + sR_p C_p}{R_n + R_p + sR_p C_p}, \quad (3.1)$$

where R_n is the sum of R_s of battery model and R_{loop} (including on-resistance of the switches, ESR of the capacitor, and resistance of sensor circuit).

By transforming the loop current into time domain, the charging current of capacitor is expressed as

$$i_1(t) = \frac{V_{OC} - v_C(t)}{R_n + R_p} \left(1 + \frac{R_p}{R_n} e^{-\frac{(R_n + R_p)t}{R_n R_p C_p}} \right), \quad (3.2)$$

3.2 EIS algorithm

In phase A ($t_0 \sim t_1$), the charge is transferred from the battery to the equalizing capacitor.

The operational principle of this phase is further analyzed as follows:

- Before each identification process, the open-circuit voltage (V_{OC}) of the battery cell is measured.

- Based on the equivalent circuit in Fig. 3.5(a), the voltage difference and the flowing current in the loop are calculated by Eq. 3.2 can be redefined by

$$\Delta V = V_{OC} - v_C(t), \quad (3.3)$$

and

$$i_1(t) = \frac{\Delta V}{R_n + R_p} \left(1 + \frac{R_p}{R_n} e^{-\frac{(R_n + R_p)t}{R_n R_p C_p}} \right), \quad (3.4)$$

3.2.1 Start and end time point strategy (S-ETPS)

The theoretical waveform in Fig. 3.6 reveal the impact of the model parameters on the capacitor current, i_C . Assuming that the polarization capacitor in battery model, C_p , is completely discharged before the beginning of phase A (t_{M1}), the battery impedance equals R_s , resulting in the highest capacitor current amplitude. At some intermediate point t_{M2} when C_p is not fully charged yet, current flows in the loop are shared between R_p and C_p , which makes the battery impedance increase. When C_p is almost fully charged at t_{M3} , charge flows mostly through R_p . By analyzing the current and voltage of equalizing capacitor, C, the model-parameter can be identified as follows:

- At $t_{M1} \cong 0$, the series resistance, R_s is calculated by

$$R_n = \frac{V_{OC} - v_c(t_{M1})}{i_1(t_{M1})}, \quad (3.5)$$

$$R_s = R_n - R_{loop}. \quad (3.6)$$

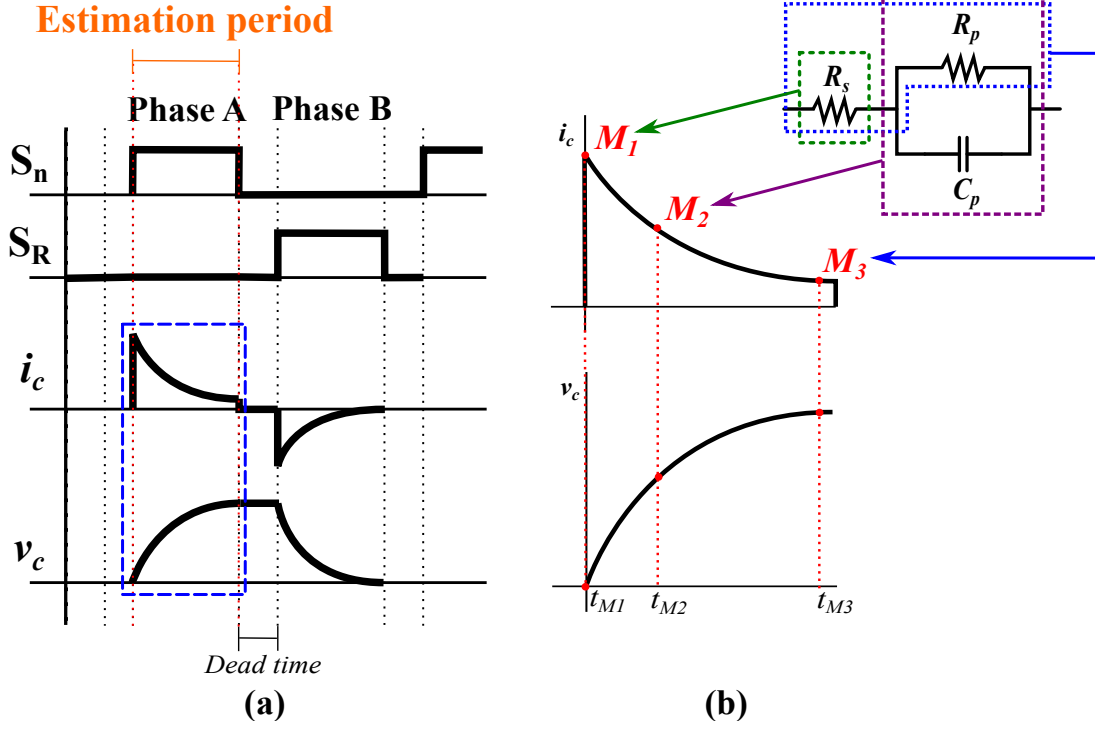


Fig. 3.6 Theoretical waveforms (a) current and voltage of the measuring capacitor; (b) start and end point strategy

- At t_{M3} which is sufficiently large, the parallel resistance, R_p , is approximately expressed as

$$R_p = \frac{V_{OC} - v_c(t_{M3})}{i_1(t_{M3})} - R_n. \quad (3.7)$$

- At t_{M2} , if we denote K as

$$K = \left(\frac{i_1(t_{M2})(R_n + R_p)}{V_{OC} - v_c(t_{M2})} - 1 \right) \frac{R_n}{R_p}, \quad (3.8)$$

the polarization capacitance, C_p , is calculated by

$$C_p = \frac{(R_n + R_p)t_{M2}}{R_n R_p \ln(\frac{1}{K})}. \quad (3.9)$$

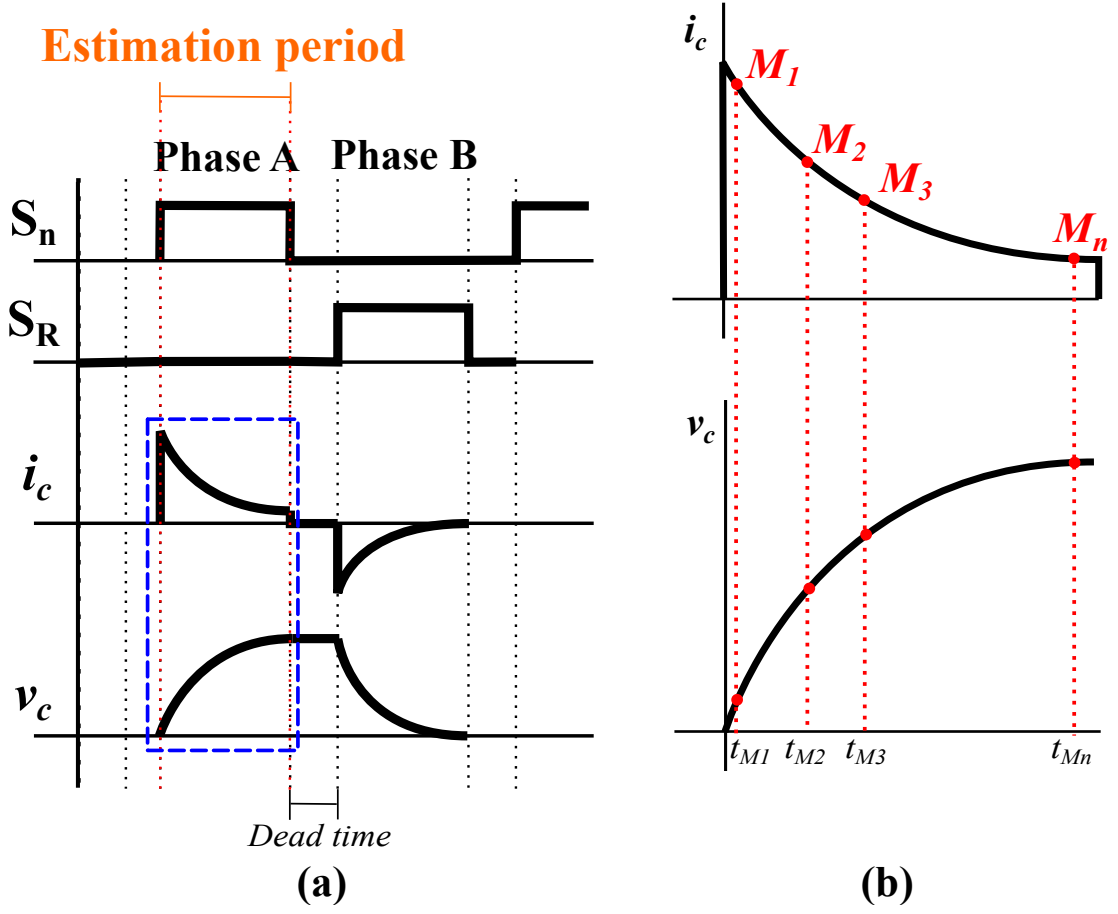


Fig. 3.7 Theoretical waveforms (a) current and voltage of the measuring capacitor; (b) multiple time point strategy

3.2.2 Multiple time point strategy (MTPS)

The theoretical waveforms of this strategy is shown in Fig. 3.7

After reformulating Eq. 3.4 into

$$\frac{i_1(t)}{\Delta V} = \frac{1}{R_n + R_p} + \frac{R_p}{R_n(R_n + R_p)} e^{-\frac{(R_n + R_p)t}{R_n R_p C_p}}, \quad (3.10)$$

and applying the exponential curve fitting to Eq. 3.10, the current (i_1) and voltage (v_c) of the equalization capacitor at the various points (Fig. 3.7) are utilized to calculate the parameters of the EIS model.

For simplicity, the parameter of Eq. 3.10 are denoted as Eq. 3.11

$$\left\{ \begin{array}{l} y = \frac{i_1(t)}{\Delta V} \\ x = t \\ a = \frac{R_p}{R_n(R_n+R_p)} \\ b = \frac{-(R_n+R_p)}{R_n R_p C_p} \\ c = \frac{1}{R_n+R_p} \end{array} \right. \quad (3.11)$$

Eq. 3.10 is reformulated into

$$y = ae^{bt} + c, \quad (3.12)$$

By measuring the current (i_1) and voltage (v_C) of the equalization capacitor at multiple time t , a set of points can be obtained $[x_1, y_1] \dots [x_n, y_n]$, At this time, 3 parameters a, b , and c can be calculated by following the below steps:

1. Calculate an approximation of b
2. Utilize b , an approximation of a is obtained
3. At this step, an approximation of c is determined

Firstly, approximation of b

Array dx holds the x differences between adjacent points $dx_1 = x_2 - x_1 \dots dx_3 = x_4 - x_3$

Array dy holds the y differences $dy_1 = y_2 - y_1 \dots dy_3 = y_4 - y_3$

Array cx holds the centers between points $cx_1 = \frac{x_1+x_2}{2} \dots cx_3 = \frac{x_3+x_4}{2}$

Array dq holds the differential quotients $dq_1 = \frac{dy_1}{dx_1} \dots dq_3 = \frac{dy_3}{dx_3}$

To eliminate c , the differentiation of $y = ae^{bx} + c$ is $y' = abe^{bx}$

Calculating the same for all sample point, the differentiations can be obtained

$$y'_1 = abe^{bx_1}$$

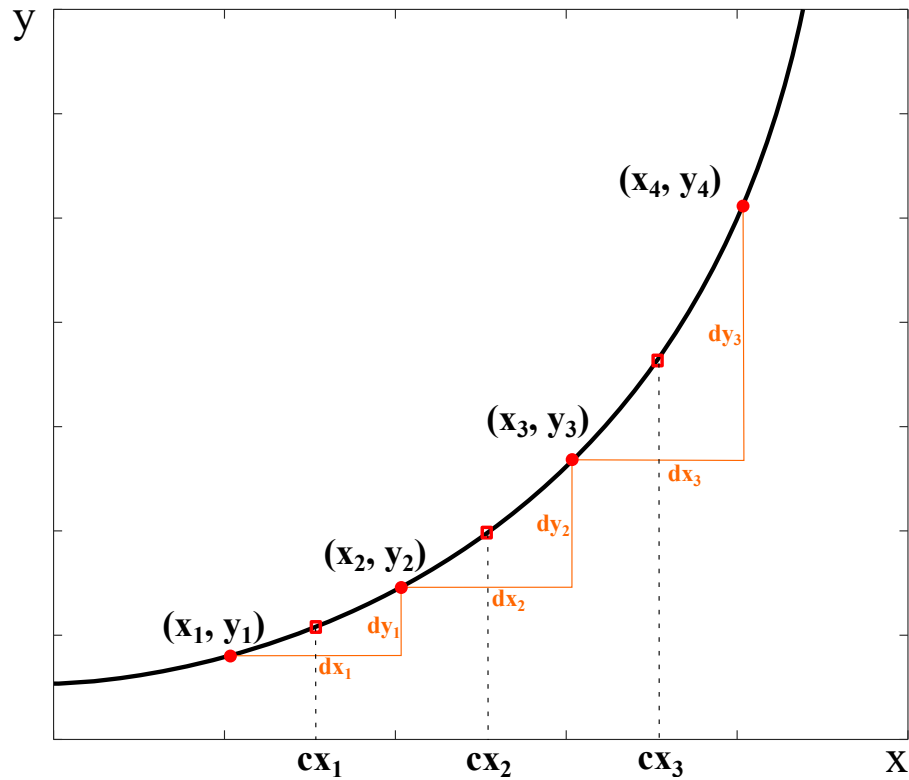


Fig. 3.8 Exponential curve fitting theory

$$y'_2 = abe^{bx_2}$$

$$y'_3 = abe^{bx_3}$$

Parameter a can be eliminated by division of subsequent y' :

$$\frac{y'_2}{y'_1} = e^{b(x_2 - x_1)}$$

$$b = \frac{\ln\left(\frac{y'_2}{y'_1}\right)}{x_2 - x_1}$$

with above arrays in mind:

$$b = \frac{\ln\left(\frac{dq_2}{dq_1}\right)}{cx_2 - cx_1}$$

$$b = \frac{\ln\left(\frac{dq_3}{dq_2}\right)}{cx_3 - cx_2} \dots$$

The center values (cx) are used, because the tangent (differential quotient dq) is most accurate between two x values. For subsequent points, the average value of b is calculated.

After calculate b , the approximation of a can be determined as follow

$$y_1 = ae^{bx_1} + c$$

$$y_2 = ae^{bx_2} + c$$

.....

c could be eliminated by subtraction of subsequent rows: $dy_1 = y_2 - y_1 = a(e^{bx_2} - e^{bx_1})$

thus

$$a = \frac{dy_1}{e^{bx_2} - e^{bx_1}}$$

$$a = \frac{dy_2}{e^{bx_3} - e^{bx_2}}$$

An average value of a is calculated.

And finally, an approximation of c is calculated by $c = y - ae^{bx}$.

3.3 Conclusion

Thévenin model is adopted as a battery model in this work. By analyzing the integrated circuit structure, the current equation of the capacitor equalizer is determined. This chapter proposed S-ETPS and MTPS current sampling strategies to determine the battery parameter. Observed that the EIS-model parameters are quickly obtained by one switching cycle. Thus, the proposed method is suitable for the online diagnosis of individual battery cells. In phase B ($t_2 \sim t_3$), a dummy load, R_{dummy} , is used to ensure that the equalizing capacitor is completely discharged before the next identification step in Fig. 3.5(b). The dummy resistance value should be carefully designed by

$$R_{dummy} \leq \frac{1}{5f_s C}, \tag{3.13}$$

where f_s is the switching frequency in the test.

Chapter 4

Proposed SOC/SOH estimation method using online model identification

4.1 Extended Kalman filter formula

According to estimating theory, the EKF is a nonlinear Kalman filter that has been improved based on a linearization technology in real-time. In the battery state estimation, the processing and system noise are approximated as white noise, which accords with Gaussian distribution [32]. It linearizes noise expectation and covariance in the estimation process.

This algorithm utilizes the input and output data of the system to determine a linear state equation to predict the present state of the system. Different from the classical algorithm, which is suitable for a linear system, EKF can apply to the discrete nonlinear system by using the Taylor series and Kalman filter algorithm. According to Eq. 4.1, the discrete nonlinear

system's expression and observation equations are provided.

$$\begin{cases} x_{k+1} &= f(x_k, k) + w_k \\ y_k &= h(x_k, k) + u_k \end{cases} \quad (4.1)$$

The state estimation is represented by the first part of Eq. (4.1) and the second part represents the observed output vector. k represents a discrete-time point; x_{k+1} denote the n -dimensional state vector. y_k is the m -dimensional observation vector. w_k and v_k are independent Gaussian white noise. To apply the Kalman filter, the first-order Taylor series expansion of nonlinear functions $f(\cdot)$ and $h(\cdot)$ is carried out around the estimated value. Consequently, the results are described as shown in Eq. 4.2.

$$\begin{cases} f(x_k, k) &\approx f(\hat{x}_k, k) + \frac{\partial f(x_k, k)}{\partial x_k} \Big|_{x_k=\hat{x}_k} (x_k - \hat{x}_k) \\ h(x_k, k) &\approx h(\hat{x}_k, k) + \frac{\partial h(x_k, k)}{\partial x_k} \Big|_{x_k=\hat{x}_k} (x_k - \hat{x}_k) \end{cases} \quad (4.2)$$

Where Jacobian matrices A_k, B_k, C_k , and D_k are expressed as Eq. 4.3.

$$\begin{cases} A_k &= \frac{\partial f(x_k, k)}{\partial x_k} \Big|_{x_k=\hat{x}_k}, \\ A_k &= f(\hat{x}_k, k) - A_k \hat{x}_k, \\ C_k &= \frac{\partial h(x_k, k)}{\partial x_k} \Big|_{x_k=\hat{x}_k}, \\ D_k &= h(\hat{x}_k, k) - C_k \hat{x}_k \end{cases} \quad (4.3)$$

Furthermore, Eq. 4.1 can be linearized as shown in Eq. 4.4.

$$\begin{cases} x_{k+1} &= A_k x_k + B_k + w_k \\ y_k &= C_k x_k + D_k + u_k \end{cases} \quad (4.4)$$

The system is linearized Eq. 4.4 in real time around the estimated state for covariance updates as the formulation Eq. 4.5.

$$\left\{ \begin{array}{l} \hat{x}_{k+1}^- = f(\hat{x}_k), \\ \hat{P}_{k+1}^- = A_k \hat{P}_k A_k^T + Q_{k+1}, \\ K_{k+1} = \hat{P}_{k+1}^- C_{k+1}^T (C_{k+1} \hat{P}_{k+1}^- C_{k+1}^T + R_{k+1})^{-1} \\ \hat{x}_{k+1} = x_{k+1}^- + K_{k+1} [y_{k+1} - h(x_{k+1}^-)], \\ \hat{P}_{k+1} = [I - K_{k+1} C_{k+1}] P_{k+1}^- \end{array} \right. \quad (4.5)$$

where k represents the number of iterations. P is the error covariance and K is the Kalman gain. Q and R are the variances of w and v , respectively. The parameter I is the identity matrix $n \times m$. The initial state value is $x(0) = E[x(0)]$, and its variance is $P(0) = Var[x(0)]$.

Besides, EKF-based battery state estimation is one of the most popular methods. However, reports indicated that these methods are sensitive to the accuracy of the battery model parameters. The influence of battery aging on the estimation accuracy is mostly neglected, even though it is significant [17, 29].

4.2 SOH estimation

To further investigate the influence of aging on the EKF estimation accuracy, multiple tests have been conducted to observe the battery characteristic at the various SOH levels. The device under test is the 18650 Li-ion Samsung SDI (3.6V/2.9Ah) cells. The cells are fully charged at 0.5C-rate current and are discharged by various C-rates (0.5C, 1.5C, and 2C) at 25°C ambient temperature. The battery cells are gradually aged by repeating the tests. After every 50 cycles, the battery impedance and OCV–SOC relationship of the cells are

observed to form the historical dataset of the cells at the various SOH levels. The changes in the battery impedance and OCV–SOC mapping curve are illustrated in Fig. 4.1 and Fig. 4.2. According to the results, the battery impedance drifted by 15% from the initial condition after 550 cycles. Meanwhile, the OCV–SOC curve deviates from the initial curve. Both factors significantly reduce the accuracy of the EKF estimation.

The same EKF estimator has been applied for the charging process of a cell at 100% and 90% SOH levels. The estimation results are compared with the reference value from the cyclers in Fig. 4.3. The maximum error increased from 2.51% (at 100% SOH) to 15.49% (at 90% SOH). Evidently, the aging of the cell increases the error of the EKF estimator. On the other hand, the aging pattern of the cells is different from each other even under the same driving condition [33]. Consequently, the assessment of the whole pack by a single EKF estimation becomes inappropriate. Therefore, online cell-by-cell state estimation is essential.

In addition, based on the historical data set of battery, the relationship between SOH level and R_t is illustrated in Fig. 4.4. The SOH level is a function of R_t , which can be derived by applying the polynomial curve fitting technique. Therefore, the SOH level is estimated directly from the measured R_t . In this work, the relation is obtained as:

$$SOH = 0.05347 \times R_t^2 - 7.138 \times R_t + 339.8. \quad (4.6)$$

where the total resistance of the cell (R_t) is calculated by

$$\Delta R_t = R_s + R_p, \quad (4.7)$$

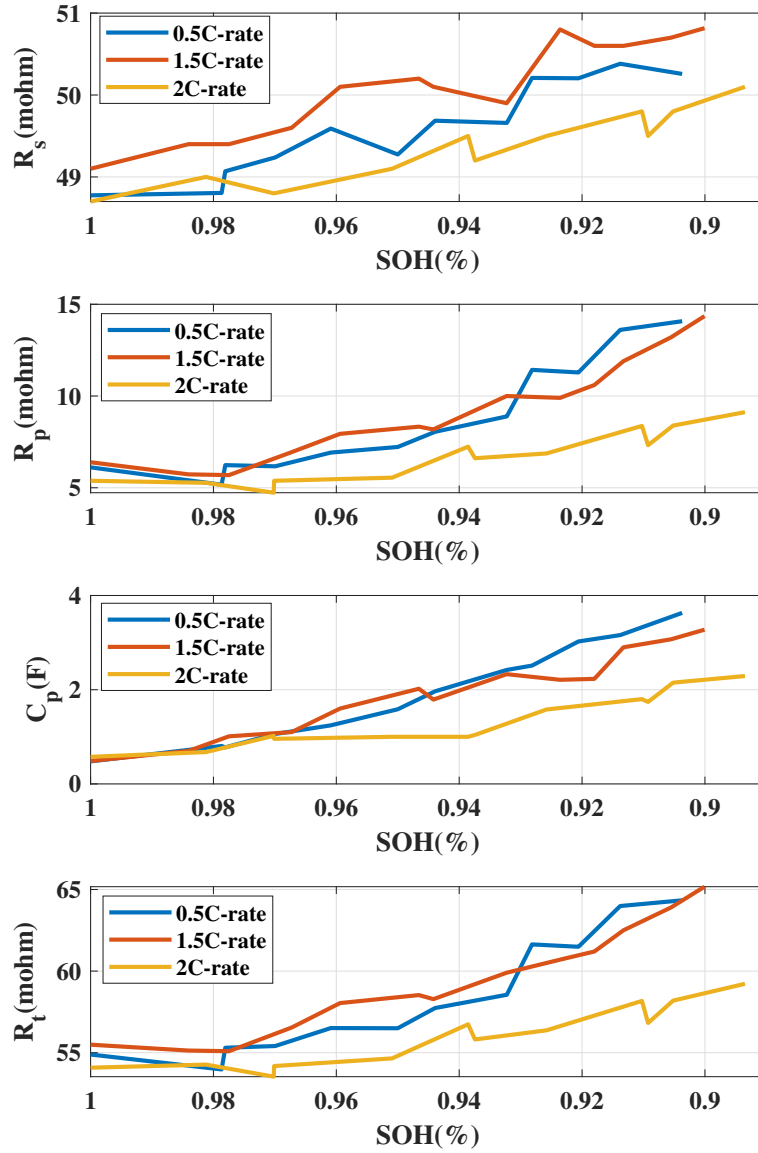


Fig. 4.1 Battery impedance change during aging

This relation is used for constructing the aging dataset look-up table, where the corresponding actual capacity (C_n) and SOC–OCV relationship are calculated based on the SOH level. Finally, the updated C_n and SOC–OCV relationship are simultaneously utilized for the EKF estimator to estimate the SOC level.

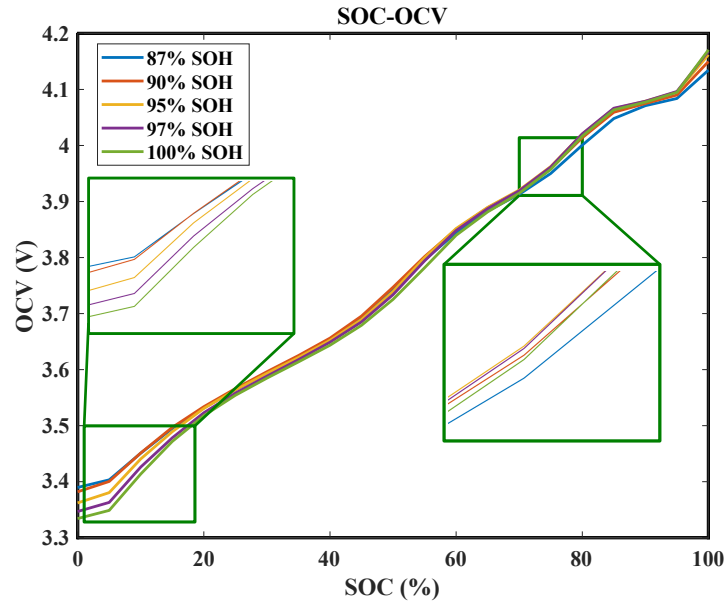


Fig. 4.2 SOC-OCV change during aging

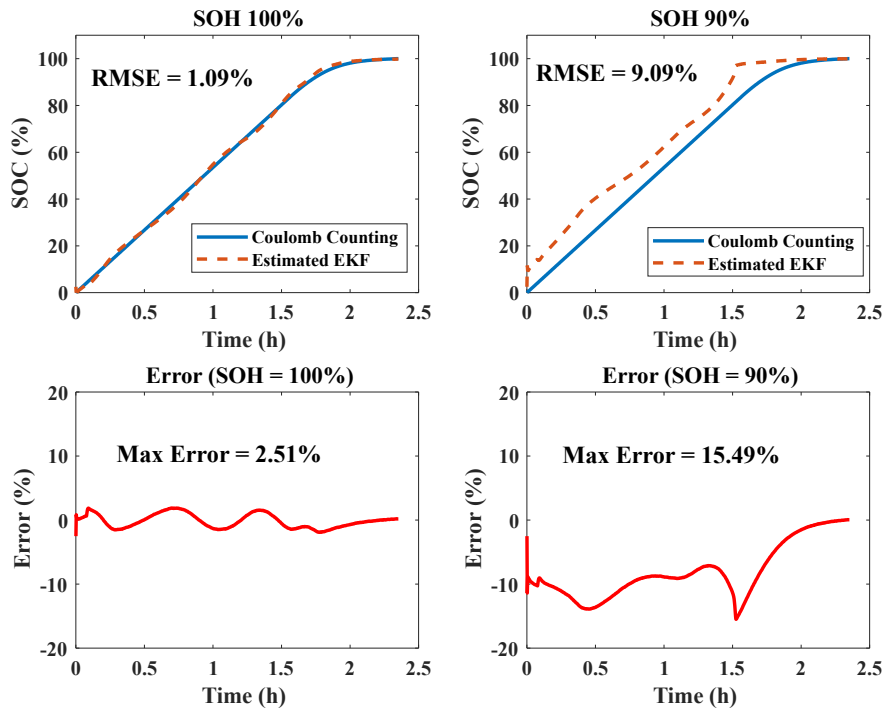


Fig. 4.3 SOC estimation without model calibration at 100% and 90% SOH

After the model parameters for one cell are obtained, the switch-matrix is controlled to dock other cells to the flying capacitor for another parameter extraction step. Because the

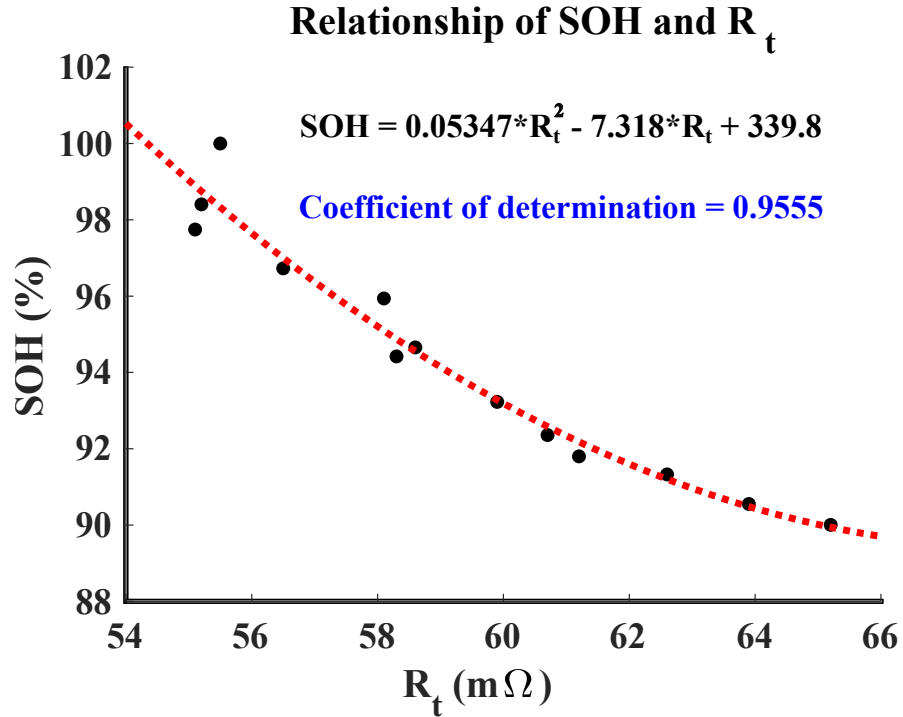


Fig. 4.4 Relationship between SOH and R_t

SOH slowly decreases by nature, this process can be conducted in the idle mode of the cells; right before every charging process or during any usual battery maintenance routine. The extra computation time or energy loss is trivial because the whole reconfiguration process is considerably fast and seldom occurs.

4.3 SOC estimation

The battery cell is modeled by a Thévenin equivalent circuit, as shown in Fig. 3.4. Although the second order model can achieve higher accuracy, its computation becomes complex. Accordingly, the first order model is chosen for the state estimation for individual cells. The model consists of an open circuit voltage (V_{OC}) and an R-RC (R_s, R_p, C_p) equivalent impedance circuit. V_{OC} is determined by LUT after updated SOC-OCV curve based on SOH levels, while the impedance is updated by the online identification as in Chapter 3. Besides,

the battery SOC can not be measured directly, instead, it should be computed by the ratio of the remaining capacity to the total capacity as

$$SOC(k+1) = SOC(k) - \frac{\eta \Delta t i(k)}{C_n} \quad (4.8)$$

Meanwhile, the terminal voltage of the cell is calculated by the first part of Eq. 4.9, and the second part is the polarization voltage

$$\begin{cases} V_{Terminal} &= V_{OC}(k) - V_P(k) - I(k)R_s \\ V_P(k+1) &= e^{\frac{-\Delta t}{R_P C_P}} V_P(k) + R_P(1 - e^{\frac{-\Delta t}{R_P C_P}})I(k) \end{cases} \quad (4.9)$$

where $V_{OC}(k)$ is the open-circuit voltage at the k th sampling time and is a function of SOC, $V_p(k)$ is the polarization voltage at the k th sampling time applied to the parallel RC network, η is the efficiency of charge/discharge process, $I(k)$ denotes the measured current of the cell, C_n is the nominal full capacity of the cell, and Δt is the sample time. For a convention, the polarity of the charging and discharging current are regarded as positive and negative, respectively.

In the battery system, the state and measurement equations can be built in as follows:

$$\begin{cases} x_{k+1} &= A_k x_k + B_k u_k \\ y_k &= C_k x_k + D_k u_k \end{cases} \quad (4.10)$$

where x_{k+1} is the state vector at time $k+1$, the state variables are $x = [SOC, V_p]$, system input is $u_k = I(k)$, and system output is $y_k = V_{Terminal}$. The A_k, B_k, C_k , and D_k matrices are given by Eq. 4.11 to Eq. 4.14 using Eq. 4.8 and Eq. 4.9:

$$A_k = \begin{bmatrix} 1 & 0 \\ 0 & e^{\frac{-\Delta t}{R_p C_P}} \end{bmatrix} \quad (4.11)$$

$$B_k = \begin{bmatrix} \frac{\eta \Delta t i(k)}{C_n} \\ R_P (1 - e^{\frac{-\Delta t}{R_p C_P}}) \end{bmatrix} \quad (4.12)$$

$$C_k = \begin{bmatrix} \frac{\partial V_{OC}}{\partial SOC} & -1 \end{bmatrix} \quad (4.13)$$

$$D_k = -R_s. \quad (4.14)$$

4.4 Conclusion

After the model parameters of the cell are identified, the EIS model is utilized to update the state space model for SOC estimation. Next, the correlation between SOH level and R_t is illustrated based on the historical dataset. The SOH level is a function of R_t , which can be derived by applying the polynomial curve fitting technique. Besides, the EKF for SOC estimation is also defined.

Chapter 5

Experimental verification

First, the reference set should be constructed. The reference SOC and SOH levels of the cells are calculated based on the actual capacity of the cells, which are provided by the Coulomb counting method with a high accuracy sensing equipment Maccor 4300K. The cell model parameters are extracted by using the sinusoidal injection method with a genetic estimation algorithm to create a reference set of data for the EIS model. This method is supplied by the commercial offline EIS measurement equipment (ZIVE SP10).

The accuracy of the model parameters is evaluated with an FPGA-based real-time hardware-in-the-loop test platform (Typhoon HIL 602+). Based on the reference parameters from the EIS test rests, the circuit model is constructed into a real-time platform to isolate the effects of unintended disturbances, such as temperature changes during the operation and manufacturing tolerances in battery characteristics. Then, the proposed method is implemented in the real-time platform, and the algorithm is executed for a 3S1P battery string consisting of three cells in series.

5.1 Battery data set

In order to collect battery data set, the test system has 3 main parts as in Fig. 5.1:

- Chamber is used for making the ambient temperature for the test.
- EIS analyzer (Zive SP10) is used to measure impedance the battery, which is placed in chamber 1.
- Cyclor equipment (Maccor 4300K) is used for cycling the batteries at 0.5C, 1.5C 2C, which is kept in chamber 2.

The test is conducted at $25^{\circ}C$ ambient temperature. 3 sample batteries are charged and discharged until SOH is smaller than 80%, and the impedance is measured every 50 cycles.

The device under test is the 18650 Li-ion Samsung SDI (3.6V/2.9Ah) cells. The specifications is shown in Table. 5.1

The experimental process is conducted according to the flowchart in Fig. 5.2

Step 1: The temperature of the chamber is set to the target temperature $25^{\circ}C$.

Step 2: The batteries are fully charged by using the CC-CV method at the current rate 0.5C (1375mA).

Step 3: At the i -th cycle so that $i\%50 == 0$ (for example: $i = 50, 100, 150, \dots$):

- Step 3.1: Set discharge rate for 4 cells is respectively set 0.5C (1375mA), 1.5C (4125mA), 2C (5500mA).
- Step 3.2: Discharge each battery in constant time t to decrease target SOC (100, 95, \dots , 0), where t (s) determined by the equation:

$$SOC = SOC(0) - \frac{\int_0^t I(t) dt}{3600 \times C} \quad (5.1)$$

5.1 Battery data set

Table 5.1 Battery Samsung INR18650-29E specifications

Item	Specification
Typical Capacity	2,850mAh (0.2C, 2.50V discharge)
Minimum Capacity	2,750mAh (0.2C, 2.50V discharge)
Charging Voltage	4.2V
Nominal Voltage	3.65V (0.2C discharge)
Charging Method	CC-CV (constant voltage with limited current)
Charging Current	Standard charge: 1,375mA
Charging Time	Standard charge: 3hours
Max. Charge Current	2,750mA (not for cycle life)
Max. Discharge Current	5,500mAh (continuous discharge) 8,250mAh (not for continuous discharge)
Discharge Cut-off Voltage	2.5V
Cell Weight	48g max
Operating Temperature (Cell Surface Temperature)	Charge : 0 to 45°C Discharge : -20 to 60°C

Corresponding to each desire SOC, let the batteries rest for 30 minutes to reach an equilibrium state. Next, measure the impedance of the battery (10kHz-0.1Hz). And repeat step 3.2 until reach cut-off voltage.

Step 4: At the i -th cycle so that $i \% 50 \neq 0$ (for example: $i \neq 50, 100, 150, \dots$), discharge rate for 3 cells is respectively set 0.5C, 1.5C, 2C. Charge/discharge in 50 cycles and logging the I, V, T, Q.

Step 5: If SOH < 80%, go to Step 3. Otherwise, the test is finished.

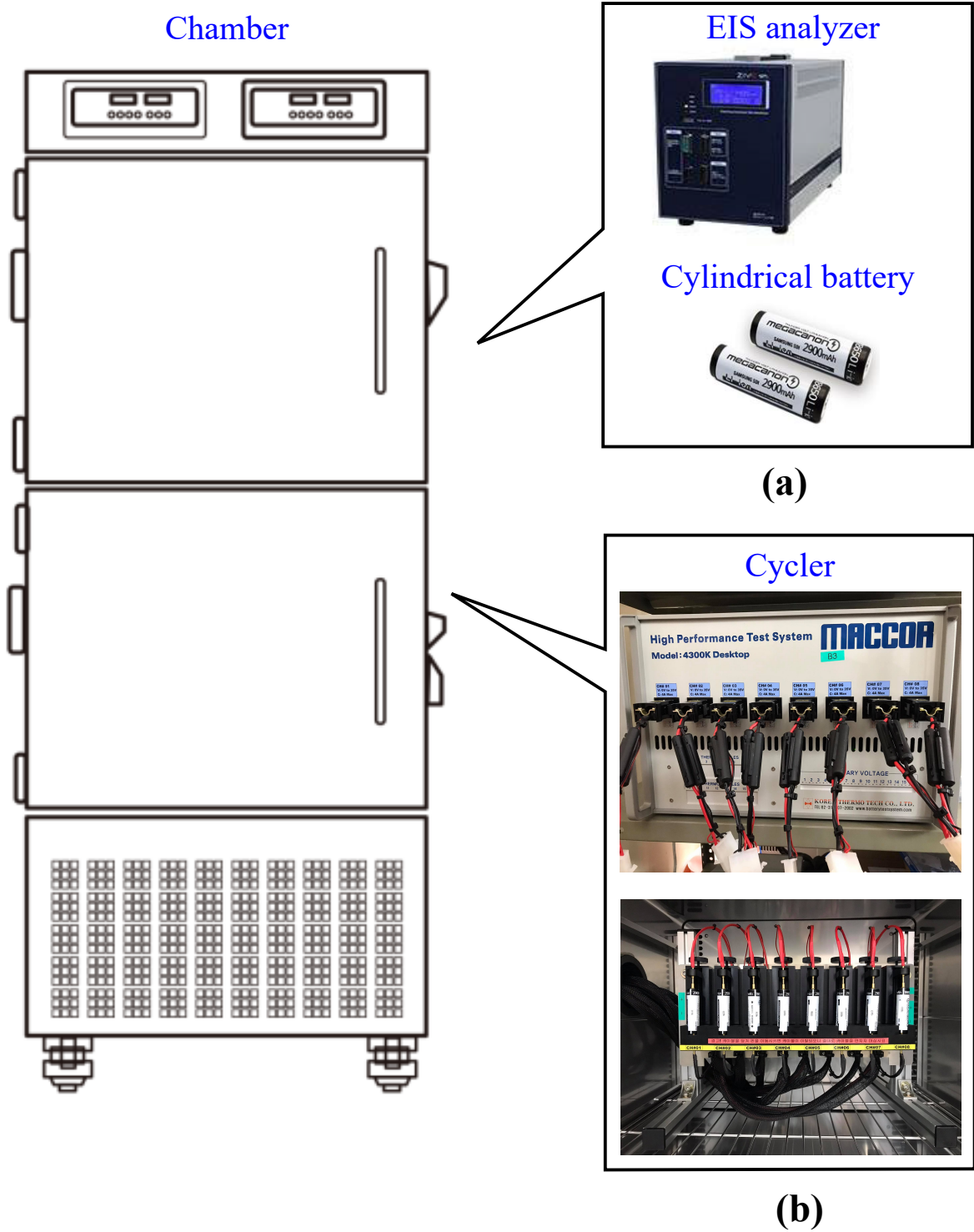


Fig. 5.1 Battery data set test set up

5.2 Validation of EIS identification

To verify the identification scheme, real-time simulations for a 3S1P 18650 Li-ion (3.6V/2.9Ah) battery string are implemented. First of all, the actual impedance of the cells is analyzed by a sinusoidal EIS equipment (Zive SP10) as a reference. Next, based on the obtained model-parameter, R-C battery model is reconstructed on a real-time simulator (Typhoon HIL602+) to exclude the effect of external factors on the battery characteristics such as temperature, pressure, etc. The setups of the other parameters are as follows: the nominal voltage of the cell is 3.6V; the equalizing capacitance is 470 μ F as it is already designed for the cell balancing circuit in [30] and R_{dummy} is designed as 20m Ω by Eq (3.13); total resistance of the loop R_n is set to 100 Ω ; switching frequency of the measurement circuit is set to 1Hz. To eliminate the measurement noise, the model-parameters are captured 5 times and the average result is used to compare the results with the measurement from the sinusoidal EIS equipment.

The waveforms of the capacitor current and voltage are shown in Fig. 5.3, all of which are similar to the theoretical analysis in Chapter 3. The model-parameter of the battery cells are estimated and summarized in Table 5.2 for S-ETPS and Table 5.3 for MTPS. The errors of the S-ETPS are within 4% for all model-parameters. For the MTPS, the estimation error is good more accurate for R_s and R_p . Although, the error becomes up to 8% for C_p , it is found that the MTPS can partially improve the model accuracy, but the number of time-point should be optimized for all three parameters. The test results indicate that the MTPS has more advantages than S-ETPS in terms of practical implementation. While the S-ETPS is sensitive to the characteristics mismatching of the cells, the MTPS can estimate the model parameters just by some arbitrary estimation point.

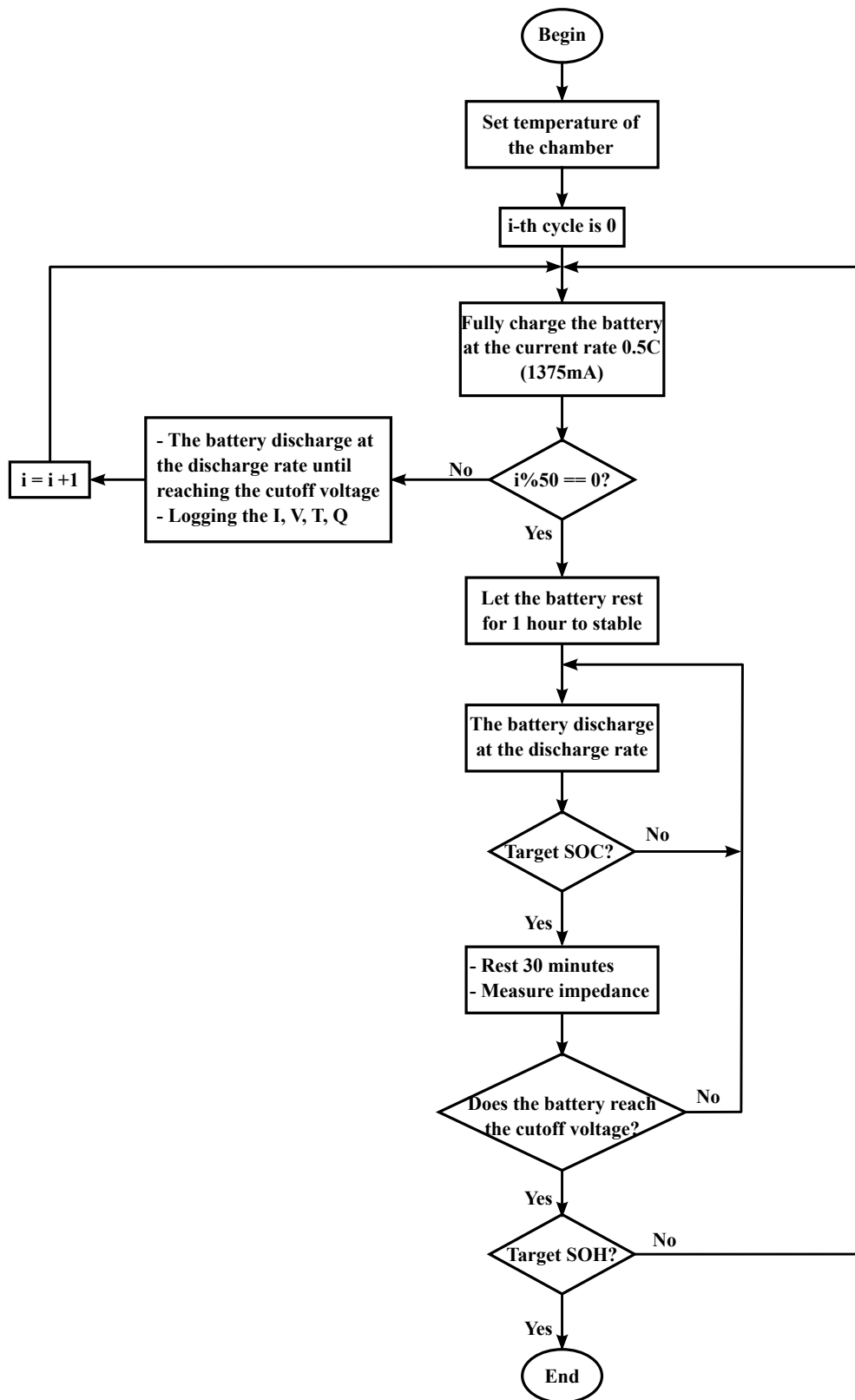


Fig. 5.2 Flow chart of the processing test

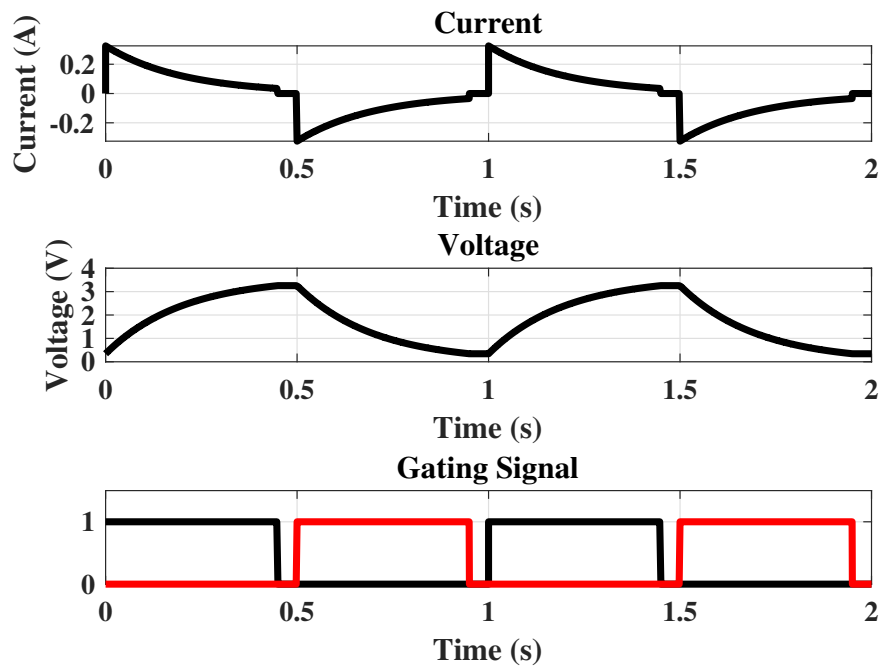


Fig. 5.3 Real time simulation result of voltage and current waveforms of equalizing capacitor

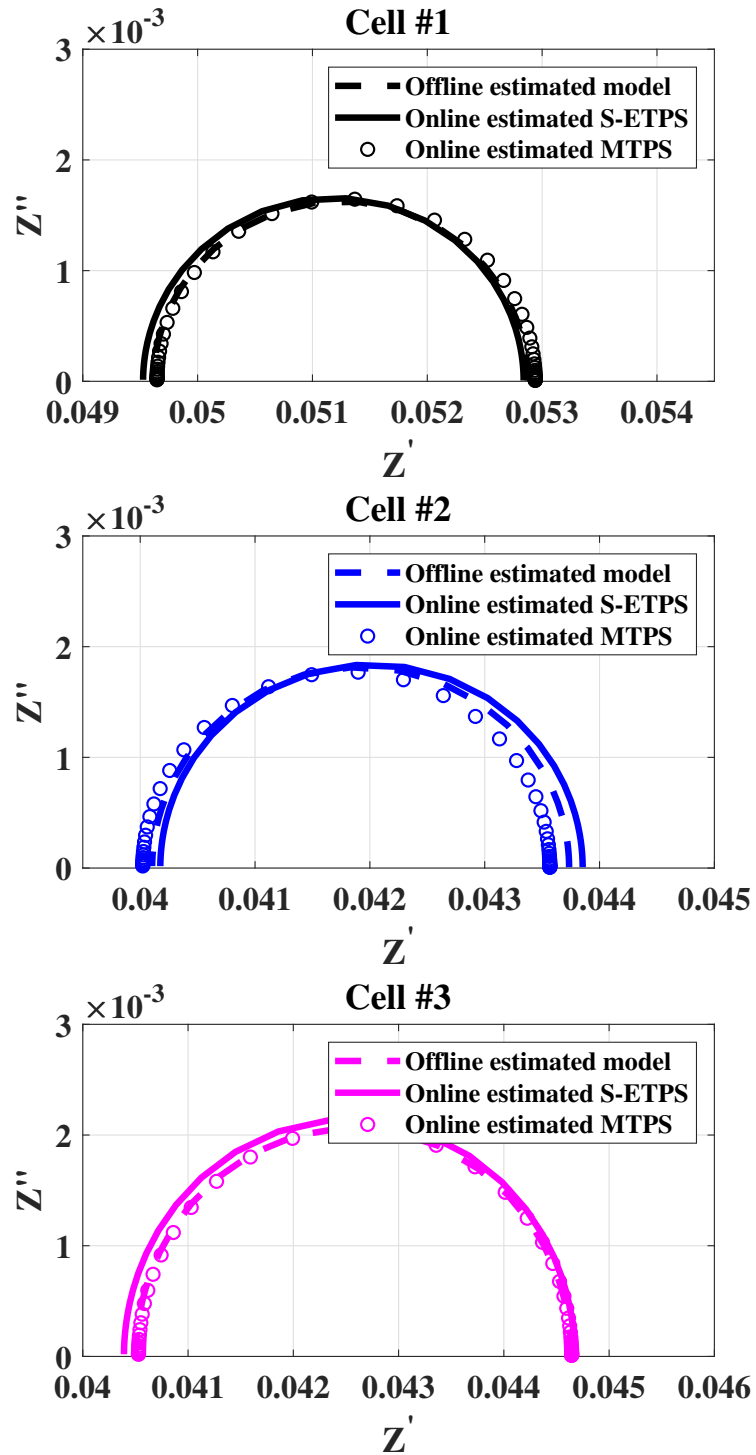


Fig. 5.4 Cole-Cole plot of the impedance: (a) cell #1; (b) cell #2; cell #3

Table 5.2 Model-parameter Identification Results of S-ETPS

	$R_s(m\Omega)$			$R_p(m\Omega)$			$C_p(F)$		
	Cell #1	Cell #2	Cell #3	Cell #1	Cell #2	Cell #3	Cell #1	Cell #2	Cell #3
Sample #1	49.629	40.123	40.527	3.312	3.693	4.245	1.125282	0.927523	0.818192
Sample #2	49.193	40.131	39.728	3.336	3.743	4.208	1.143	0.9208	0.8212
Sample #3	49.533	40.034	40.83	3.265	3.629	4.32	1.141	0.9223	0.8052
Sample #4	50.055	40.777	39.727	3.32	3.644	4.313	1.1285	0.9283	0.8029
Sample #5	49.214	39.808	41.144	3.34	3.682	4.323	1.106	0.9417	0.8333
Average	49.525	40.175	40.391	3.314	3.678	4.282	1.129	0.9281	0.8162
Actual value	49.617	40.104	40.504	3.258	3.631	4.136	1.117	0.916347	0.79933
Error (%)	-0.185	0.177	-0.279	1.719	1.294	3.530	1.074	1.283	2.111

Table 5.3 Model-parameter Identification Results of MPTS

	$R_s(m\Omega)$			$R_p(m\Omega)$			$C_p(F)$		
	Cell #1	Cell #2	Cell #3	Cell #1	Cell #2	Cell #3	Cell #1	Cell #2	Cell #3
Sample #1	49.97	39.867	40.235	3.269	3.529	4.117	1.157058	0.848248	0.832647
Sample #2	49.291	40.03	40.477	3.318	3.567	4.124	1.161163	0.853121	0.822969
Sample #3	49.477	40.265	40.668	3.306	3.515	4.15	1.16982	0.848962	0.829309
Sample #4	49.682	40.273	40.622	3.286	3.526	4.108	1.160615	0.84106	0.822909
Sample #5	49.811	39.676	40.642	3.291	3.588	4.076	1.146344	0.833609	0.817165
Average	49.646	40.022	40.529	3.294	3.545	4.115	1.159	0.845	0.825
Actual value	49.617	40.104	40.504	3.258	3.631	4.136	1.117	0.916347	0.79933
Error (%)	0.059	-0.204	0.061	1.105	-2.368	-0.508	3.760	-7.786	3.211

To assess the frequency response of the equivalent circuit using estimated model-parameters, the Cole-Cole plot of the conventional multi-frequency sinusoidal sweep test, reference model generated by conventional single frequency sinusoidal test, and model constructed by the proposed online method are illustrated in Fig. 5.4. The curves show that the difference between the reference model and the estimation is trivial. Thus, it is demonstrated that the proposed scheme can re-enact the EIS-model just by one equalization cycle at a single operating frequency.

Because the frequency-sweep is excluded, the execution time is significantly reduced. The proposed scheme only requires about a few seconds to identify the EIS-model of one battery, while the commercial equipment takes more than 2 minutes. On the other hand, the computation complexity is low enough that it can be handled by a low-cost MCU. It means that the proposed scheme has a high potential to be applied for multiple cell applications.

5.3 Validation of SOH/SOC estimation

After constructing the reference set, the reference SOC and SOH levels of the cells are calculated based on the actual capacity of the cells, which are provided by the Coulomb counting method. Based on the EIS test result in Section 5.2, the circuit model is constructed into a real-time platform to isolate the effects of unintended disturbances, such as temperature changes during the operation and manufacturing tolerances in battery characteristics. Then, the proposed method is implemented in the real-time platform, and the MPTS is executed for a 3S1P battery string consisting of three cells in series. The estimated parameters are summarized in Table. 5.4.

According to the comparison of the extracted parameters with the reference value from the commercial EIS equipment, the maximum errors in the estimation are 0.12% for R_s , 3.18% for R_p , 0.7% for R_t , and 3.54% for C_p , respectively. Thus, the EKF parameters, such as R_s , R_p , and C_p , can be successively reconfigured.

Meanwhile, the actual SOH level is predicted by the proposed algorithm based on the estimated impedance of the cells and the data set. The predicted values are summarized in Table. 5.5, where the proposed method can predict the SOH level within 1.2% error, showing that the proposed method efficiently performs in predicting the SOH condition of the cells. In this case, the remaining EKF parameters, such as OCV–SOC relation and C_n , can be obtained.

Thenceforth, EKF parameters reflect the aging effects, and the SOC estimation accuracy is greatly improved. To closely investigate the performance, the EKF estimation with or without the state space parameters reconfiguration is tested for a 0.5C-rate charging and 1.5C-rate discharging process at the 100th (97.75% SOH), 400th (92.36% SOH), 550th cycle (91.3% SOH). The SOC estimation error is assessed by root-mean-square-error (RMSE), which is calculated by

$$RMSE = \sqrt{\frac{\sum_{i=1}^N (SOC_{ref} - SOC_{estimated})^2}{N}} \quad (5.2)$$

where SOC_{ref} and $SOC_{estimated}$ are the reference SOC and the estimated SOC, respectively; and N is the number of data. The terminal voltage and SOC profile of the battery cell are illustrated in Fig. 5.5, Fig. 5.6, Fig. 5.7. The EKF estimation without the aging consideration has a high RMSE in SOC estimation and RMSE increase during battery aging (the lowest RMSE at 250th cycle and the highest RMSE at 900th cycle). By contrast, the

estimation error is reduced below 1.63% RMSE because the model parameter is extracted on-line and cell-by-cell. Therefore, the state space parameter reconfiguration process is effective in improving the accuracy of the SOC estimation for individual cells.

5.4 Conclusion

The experiment was conducted to collect data set at $25^{\circ}C$ ambient temperature. The parameter identification results based on hardware in the loop are compared. The results indicate that MTPS has more advantages in practical implementation. The results of the SOC/SOH estimation demonstrate the efficiency of the state space parameter reconfiguration process in increasing the precision of the SOC estimation for individual cells within 1.63% RMSE.

Table 5.4 Model-parameter Identification Results for 3 cells

	Cell #1				Cell #2				Cell #3			
	$R_s(m\Omega)$	$R_p(m\Omega)$	$R_t(m\Omega)$	$C_p(F)$	$R_s(m\Omega)$	$R_p(m\Omega)$	$R_t(m\Omega)$	$C_p(F)$	$R_s(m\Omega)$	$R_p(m\Omega)$	$R_t(m\Omega)$	$C_p(F)$
Sample #1	49.113	5.636	55.214	1.032	51.689	10.112	61.838	2.132	49.909	11.416	61.907	2.875
Sample #2	50.051	5.700	54.963	1.012	49.939	10.042	61.928	2.150	50.958	11.445	62.758	2.920
Sample #3	48.751	5.594	54.056	1.042	50.131	9.867	60.783	2.102	50.978	11.548	63.158	2.881
Sample #4	49.229	5.677	54.379	1.037	51.451	9.973	61.248	2.146	49.864	11.784	63.149	2.892
Sample #5	49.847	5.712	54.699	1.025	50.847	9.854	59.725	2.134	50.661	11.399	62.319	2.867
Average	49.400	5.700	55.100	1.028	50.734	10.032	60.766	2.132	50.545	11.570	62.115	2.868
Actual value	49.432	5.690	55.121	1.009	50.754	9.899	60.653	2.210	50.606	11.950	62.556	2.897
Error (%)	-0.0642	0.1810	-0.0389	1.8735	-0.0389	1.3415	0.1864	-3.5446	-0.1206	-3.1793	-0.7049	-1.0209

Table 5.5 SOH estimation result by proposed method

	$R_{t-reference}(m\Omega)$	$R_{t-estimated}(m\Omega)$	$SOH_{ref}(\%)$	$SOH_{estimated}(\%)$	$SOH_{error}(\%)$
Cell #1	55.12144	55.1	97.74741	98.9137	1.1931
Cell #2	60.65297	60.766	92.35813	92.5527	0.2107
Cell #3	62.55597	62.115	91.32608	91.5443	0.2389

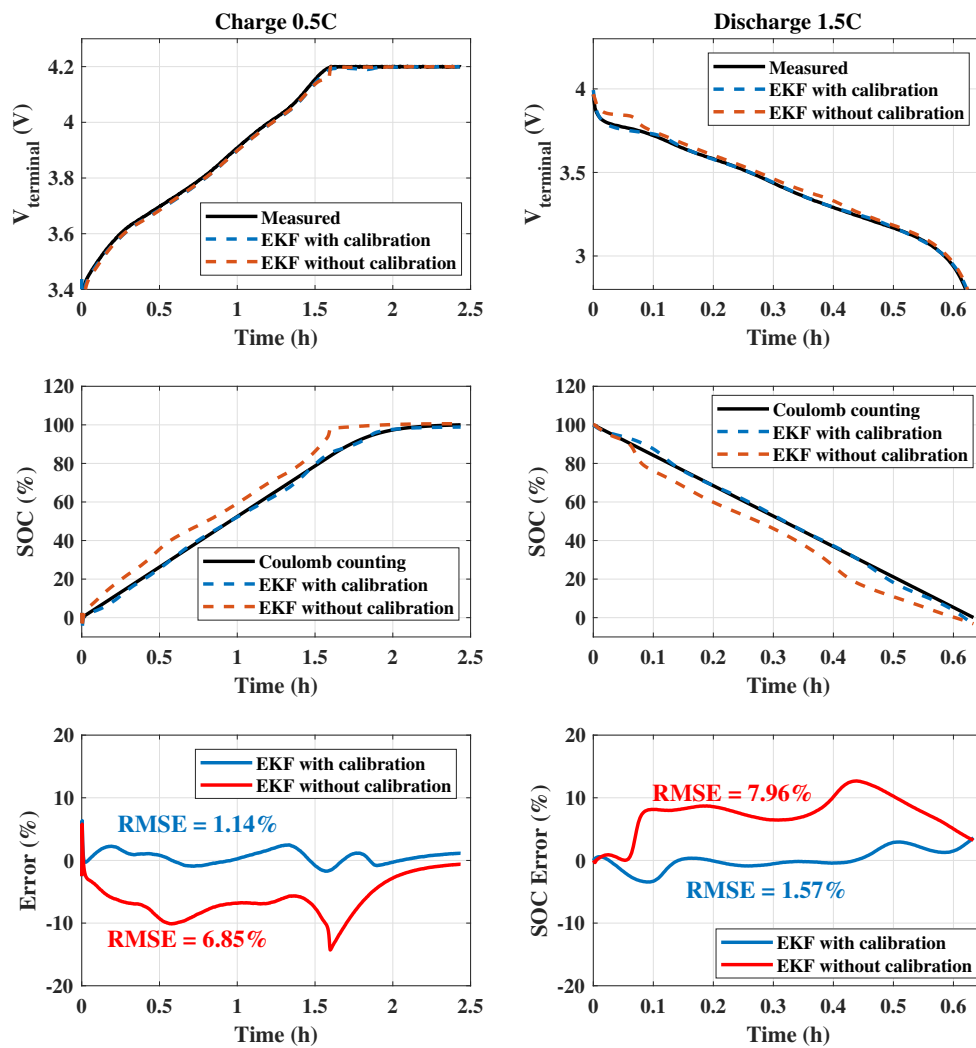


Fig. 5.5 SOC estimation result at 97.75% SOH

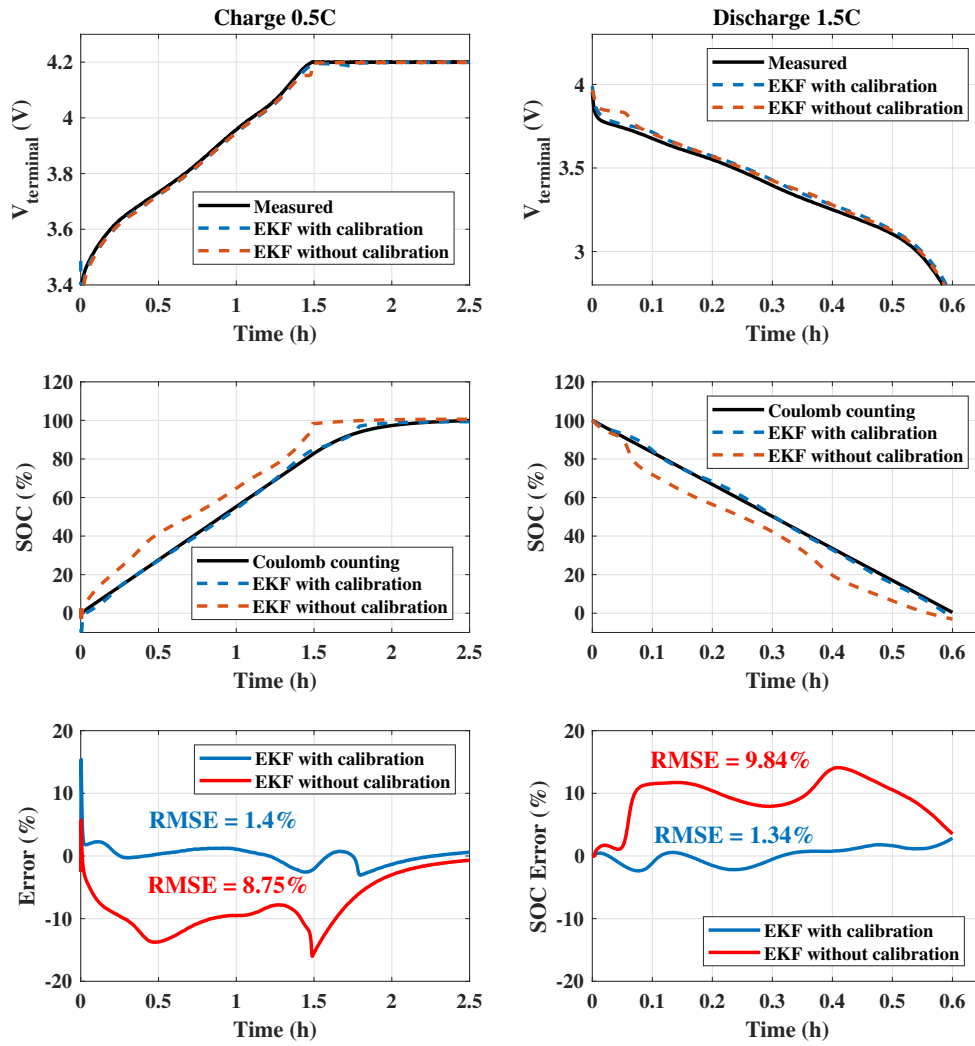


Fig. 5.6 SOC estimation result at 92.36% SOH

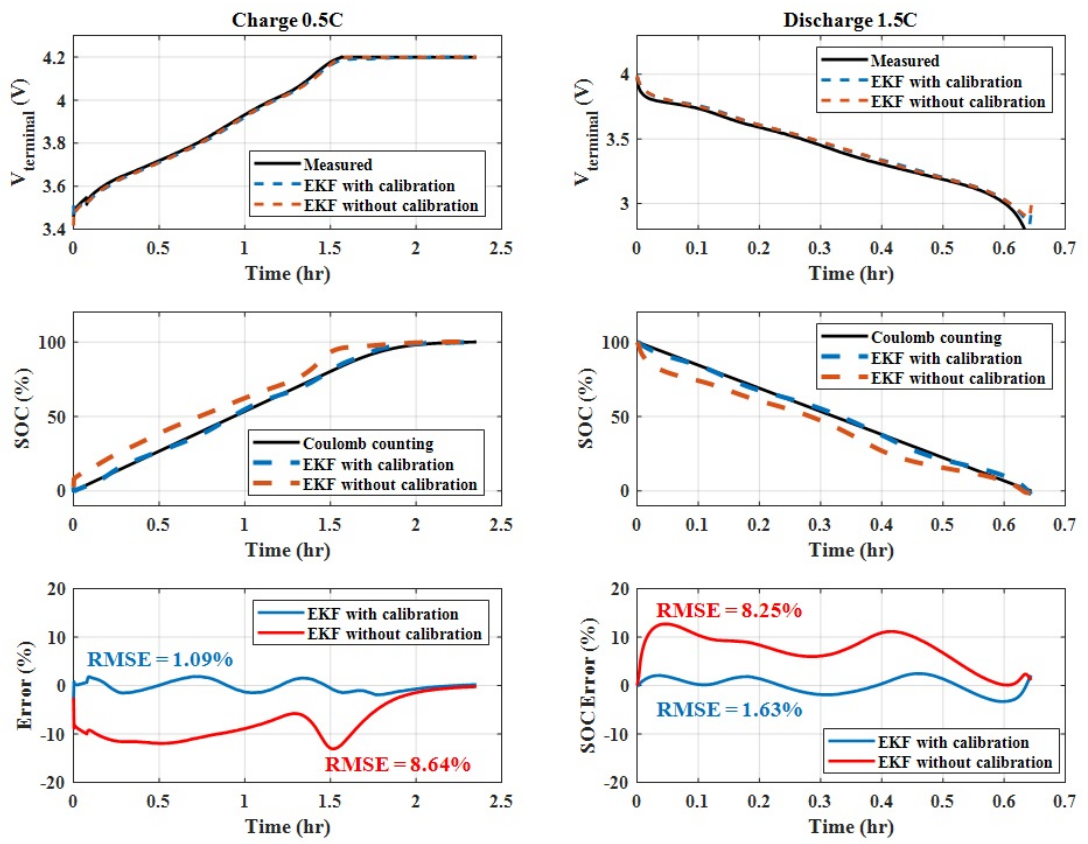


Fig. 5.7 SOC estimation result at 91.3% SOH

Chapter 6

Conclusion and future work

6.1 Conclusion

As stated in chapter Introduction, the battery state of individual cells should be monitored by considering the aging characteristics of the individual cell rather than a whole battery module or pack. Since individual cells are operating in different cooling profiles and the aging patterns of the cells are dissimilar from each other, estimation results for the whole battery module or pack mostly fail to represent the state of individual cells. This kind of problem becomes more severe in the second-life battery system. At this time, individual cell characteristics are not as uniform as the new one. For that reason, the mismatch in the battery characteristics can make the series string suffer from over-charging and over-discharging. A calibration method for SOC estimation using EKF was presented in this thesis. In the proposed method, the online cell-by-cell parameter extraction technique for the individual cell is proposed along with a switch matrix flying capacitor structure by considering the battery aging. The SOC and SOH levels are obtained by tracking the actual model parameters of the individual cells. The verification result proves that the EKF estimation combined

with the proposed state space parameter reconfiguration process can effectively improve the estimation accuracy. Furthermore, the proposed circuit structure is simple enough to be integrated into conventional active cell balancing circuits.

6.2 Future work

The field of BMS is not the only trend these days but also involved in many disciplines. The work presented in this thesis is but a small part of the required effort. The following is a summary of some recommendations for additional study.

- In this work, the model accuracy of the MTPS is dependent on the sampling times. To improve the model accuracy, the number of time-point should be considered and optimized.
- Besides, the proposed method depends on the capacitor equalizer structure. Developing a general algorithm to identify the parameters of the battery is necessary. This algorithm could be applied to any equalizer structure to determine the battery model for an individual cell.
- In addition, this thesis did not consider the thermal model of the battery. In the future, the combination of aging and thermal model is necessary because the battery is always operated at different ambient temperatures. This issue also causes the mismatching of battery characteristics.

Biography

Ngoc-Thao Pham received a B.S Degree in Electrical Engineering in 2019 - from the Ho Chi Minh City University of Technology (HCMUT) - Vietnam National University, Ho Chi Minh City, Vietnam. After graduating, she worked for Greystone Data System Vietnam as a Software engineer. Now, she is studying for the Master's program. Her current research interests include Battery Management Systems (BMS): EIS model identification for battery, Battery state estimation. Email: ptnthao1776@gmail.com

Journals

- [1] N.-T. Pham, P.-H. La, and S.-J. Choi, "Online cell-by-cell SOC/SOH estimation method for battery module employing extended Kalman filter algorithm with aging effect consideration," *Journal of Power Electronics*, pp. 1–8, 2022.

Conferences

- [2] N.-T. Pham, P.-H. La, and S.-J. Choi, "Online Model-Parameter Identification for Battery Cells Utilizing Switched-Capacitor Equalizers," in *2022 IEEE Applied Power Electronics Conference and Exposition (APEC)*, pp. 1-6, 2022.

- [3] N.-T. Pham, P.-H. La, and S.-J. Choi, "Comparison of Different Current Sampling Strategies for an Online Battery Model Identification using Switched-Capacitor Equalizer," *In proceedings of the KIFE Conference*, pp. 117–118, 2021.

References

- [1] J. Zhang, X.-G. Yang, F. Sun, Z. Wang, and C.-Y. Wang, “An online heat generation estimation method for lithium-ion batteries using dual-temperature measurements,” *Applied Energy*, vol. 272, p. 115262, 2020.
- [2] H. Yuan, H. Dai, X. Wei, and P. Ming, “Model-based observers for internal states estimation and control of proton exchange membrane fuel cell system: A review,” *Journal of Power Sources*, vol. 468, p. 228376, 2020.
- [3] G. A. L. Castillo, L. A. C. Alava, W. M. S. Arauz, and J. A. P. Rodríguez, “Proposal of photovoltaic system for house,” *International Journal of Physical Sciences and Engineering*, vol. 4, no. 2, pp. 26–35, 2020.
- [4] M. Zhang, K. Wang, and Y.-t. Zhou, “Online state of charge estimation of lithium-ion cells using particle filter-based hybrid filtering approach,” *Complexity*, vol. 2020, 2020.
- [5] J. Kim and B. Cho, “Screening process-based modeling of the multi-cell battery string in series and parallel connections for high accuracy state-of-charge estimation,” *Energy*, vol. 57, pp. 581–599, 2013.

-
- [6] H. Dong, W. Huang, and Y. Zhao, “Low complexity state-of-charge estimation for lithium-ion battery pack considering cell inconsistency,” *Journal of Power Sources*, vol. 515, p. 230599, 2021.
- [7] R. Guo, L. Lu, M. Ouyang, and X. Feng, “Mechanism of the entire overdischarge process and overdischarge-induced internal short circuit in lithium-ion batteries,” *Scientific reports*, vol. 6, p. 30248, 2016.
- [8] C. Zhang, Y. Jiang, J. Jiang, G. Cheng, W. Diao, and W. Zhang, “Study on battery pack consistency evolutions and equilibrium diagnosis for serial-connected lithium-ion batteries,” *Applied Energy*, vol. 207, pp. 510–519, 2017.
- [9] E. Martinez-Laserna, I. Gandiaga, E. Sarasketa-Zabala, J. Badedo, D.-I. Stroe, M. Swierczynski, and A. Goikoetxea, “Battery second life: Hype, hope or reality? a critical review of the state of the art,” *Renewable and Sustainable Energy Reviews*, vol. 93, pp. 701–718, 2018.
- [10] Y. Chen, Y. Kang, Y. Zhao, L. Wang, J. Liu, Y. Li, Z. Liang, X. He, X. Li, N. Tavajohi *et al.*, “A review of lithium-ion battery safety concerns: The issues, strategies, and testing standards,” *Journal of Energy Chemistry*, vol. 59, pp. 83–99, 2021.
- [11] S. Park, J. Ahn, T. Kang, S. Park, Y. Kim, I. Cho, and J. Kim, “Review of state-of-the-art battery state estimation technologies for battery management systems of stationary energy storage systems,” *Journal of Power Electronics*, vol. 20, no. 6, pp. 1526–1540, 2020.
- [12] R. Xiong, J. Cao, Q. Yu, H. He, and F. Sun, “Critical review on the battery state of charge estimation methods for electric vehicles,” *Ieee Access*, vol. 6, pp. 1832–1843, 2017.

-
- [13] K. S. Ng, C.-S. Moo, Y.-P. Chen, and Y.-C. Hsieh, “Enhanced coulomb counting method for estimating state-of-charge and state-of-health of lithium-ion batteries,” *Applied energy*, vol. 86, no. 9, pp. 1506–1511, 2009.
- [14] L. Zhao, M. Lin, and Y. Chen, “Least-squares based coulomb counting method and its application for state-of-charge (soc) estimation in electric vehicles,” *International Journal of Energy Research*, vol. 40, no. 10, pp. 1389–1399, 2016.
- [15] A. J. Salkind, C. Fennie, P. Singh, T. Atwater, and D. E. Reisner, “Determination of state-of-charge and state-of-health of batteries by fuzzy logic methodology,” *Journal of Power sources*, vol. 80, no. 1-2, pp. 293–300, 1999.
- [16] G. L. Plett, “Extended kalman filtering for battery management systems of lipb-based hev battery packs: Part 3. state and parameter estimation,” *Journal of Power sources*, vol. 134, no. 2, pp. 277–292, 2004.
- [17] V. Pop, H. Bergveld, P. P. Regtien, J. O. het Veld, D. Danilov, and P. Notten, “Battery aging and its influence on the electromotive force,” *Journal of The Electrochemical Society*, vol. 154, no. 8, p. A744, 2007.
- [18] M. Kim, K. Kim, J. Kim, J. Yu, and S. Han, “State of charge estimation for lithium ion battery based on reinforcement learning,” *IFAC-PapersOnLine*, vol. 51, no. 28, pp. 404–408, 2018.
- [19] G. You, X. Wang, C. Fang, S. Zhang, and X. Hou, “State of charge estimation of lithium-ion battery based on double deep q network and extended kalman filter,” in *IOP Conference Series: Earth and Environmental Science*, vol. 615, no. 1. IOP Publishing, 2020, p. 012080.

-
- [20] I. E. Agency. Global ev outlook 2020. [Accessed July 26, 2020]. [Online]. Available: <https://webstore.iea.org/global-ev-outlook-2020>
- [21] M. Weil and S. Ziemann, “Recycling of traction batteries as a challenge and chance for future lithium availability,” in *Lithium-Ion Batteries*. Elsevier, 2014, pp. 509–528.
- [22] T. R. Hawkins, B. Singh, G. Majeau-Bettez, and A. H. Strømman, “Comparative environmental life cycle assessment of conventional and electric vehicles,” *Journal of industrial ecology*, vol. 17, no. 1, pp. 53–64, 2013.
- [23] X. Gong, R. Xiong, and C. C. Mi, “Study of the characteristics of battery packs in electric vehicles with parallel-connected lithium-ion battery cells,” *IEEE Transactions on Industry Applications*, vol. 51, no. 2, pp. 1872–1879, 2014.
- [24] B.-Y. Chang and S.-M. Park, “Electrochemical impedance spectroscopy,” *Annual Review of Analytical Chemistry*, vol. 3, pp. 207–229, 2010.
- [25] L. Lu, X. Han, J. Li, J. Hua, and M. Ouyang, “A review on the key issues for lithium-ion battery management in electric vehicles,” *Journal of power sources*, vol. 226, pp. 272–288, 2013.
- [26] W. Shen, C. Chan, E. Lo, and K. Chau, “A new battery available capacity indicator for electric vehicles using neural network,” *Energy Conversion and Management*, vol. 43, no. 6, pp. 817–826, 2002.
- [27] T. Hansen and C.-J. Wang, “Support vector based battery state of charge estimator,” *Journal of Power Sources*, vol. 141, no. 2, pp. 351–358, 2005.

- [28] C. Pulavarthi, R. Kalpana, and P. Parthiban, “State of charge estimation in lithium-ion battery using model based method in conjunction with extended and unscented kalman filter,” in *2020 International Conference on Power Electronics and Renewable Energy Applications (PEREA)*, 2020, pp. 1–6.
- [29] R. Xiong, Y. Pan, W. Shen, H. Li, and F. Sun, “Lithium-ion battery aging mechanisms and diagnosis method for automotive applications: Recent advances and perspectives,” *Renewable and Sustainable Energy Reviews*, vol. 131, p. 110048, 2020.
- [30] P.-H. La, H.-H. Lee, and S.-J. Choi, “A single-capacitor equalizer using optimal pairing algorithm for series-connected battery cells,” in *2019 IEEE Energy Conversion Congress and Exposition (ECCE)*. IEEE, pp. 5078–5083.
- [31] A. Seaman, T.-S. Dao, and J. McPhee, “A survey of mathematics-based equivalent-circuit and electrochemical battery models for hybrid and electric vehicle simulation,” *Journal of Power Sources*, vol. 256, pp. 410–423, 2014.
- [32] S. Wang, C. Fernandez, Y. Chunmei, F. Yongcun, C. Wen, D.-I. Stroe, and Z. Chen, *Battery System Modeling*. Elsevier, 2021.
- [33] X. Gong, R. Xiong, and C. C. Mi, “Study of the characteristics of battery packs in electric vehicles with parallel-connected lithium-ion battery cells,” *IEEE Transactions on Industry Applications*, vol. 51, no. 2, pp. 1872–1879, 2014.